land

MDPI

*Article*

# Evolution of Deep-Seated Gravitational Slope Deformations in Relation with Uplift and Fluvial Capture Processes in Central Eastern Sardinia (Italy)

**Valentino Demurtas *, Paolo Emanuele Orrù and Giacomo Deiana**

Department of Chemical and Geological Sciences, University of Cagliari, 09042 Monserrato, Italy; orrup@unica.it (P.E.O.); giacomo.deiana@unica.it (G.D.)
* Correspondence: valentino.demurtas@unica.it

**Abstract:** Connections between Plio-Pleistocenic tectonic activity and geomorphological evolution were studied in the Pardu Valley and Quirra Valley (Ogliastra, East Sardinia). The intensive Quaternary tectonic activity in Sardinia linked to the opening of the Tyrrhenian Basin is known. In Eastern Sardinia, it manifests with an uplift that is recorded by geomorphological indicators, such as deep-seated gravitational slope deformation, fluvial captures, engraved valleys, waterfalls, and heterogeneous water drainage. The Pardu River flows from the NW toward the SE and then abruptly changes direction toward the NE. At this point, a capture elbow adjacent to the current head of the Quirra River is well developed. The Quirra River, in its upstream part, flows at altitudes approximately 200 m higher than the Pardu River. It also shows an oversized and over-flooded valley with respect to the catchment area upstream. This setting indicates that the Pardu River, which previously flowed south along the Quirra River, was captured by the Pelau River. We analyzed long-term landslides with lateral spreading and sackung characteristics, which involve giant carbonate blocks and underlying foliated metamorphites in both valleys. The use of LiDAR, high-resolution uncrewed aerial vehicle digital photogrammetry (UAV-DP), and geological, structural, and geomorphological surveys enabled a depth morphometric analysis and the creation of interpretative 3D models of DGSDs. Space-borne interferometric synthetic aperture radar (InSAR) data using ERS and Sentinel-1 satellites identified downslope movement of up to 20 mm per year in both Pardu Valley flanks. Multi-source and multi-scale data showed that the state of activity of the DGSDs is closely linked to the geomorphological evolution of the catchment areas of the Rio Pardu and Rio Quirra. The intense post-capture erosion acted in the Rio Pardu Valley, giving it morphometric characteristics that were favorable to the current evolution of the DGSDs, while the Rio Quirra Valley presents paleo-DGSDs that have been fossilized by pre-capture terraced alluvial deposits.

**Keywords:** morphotectonic; morphostratigraphy; DGSDs; river capture; fluvial terraces; Sardinia; Italy



**Citation:** Demurtas, V.; Orrù, P.E.; Deiana, G. Evolution of Deep-Seated Gravitational Slope Deformations in Relation with Uplift and Fluvial Capture Processes in Central Eastern Sardinia (Italy). *Land* **2021**, *10*, 1193. https://doi.org/10.3390/land10111193

Academic Editor: Giulio Iovine

Received: 15 October 2021
Accepted: 3 November 2021
Published: 5 November 2021



## 1. Introduction

The Pliocene and Quaternary geodynamic processes related to the Tyrrhenian basin opening led an uplift in Sardinia [1–3]. This is evidenced by a morphotectonic setting linked to fluvial and gravitative morphologies [4,5]. Therefore, the hydrographic basins of the Rio Quirra and the Rio Pardu have been studied in detail in order to analyze their evolutionary scenarios in relation to a river capture.

Rio Pardu and Rio Quirra are two of the most important rivers in central eastern Sardinia. The two basins are separated by a river capture caused by the Rio Pelau, which isolated Rio Pardu, the catchment area of Rio Quirra. Rio Pardu flows from northwest to southeast and then flows towards the northeast through a river capture elbow with the name of Rio Pelau. Rio Quirra flows from the north to the south parallel to the coast and then abruptly bends towards the Tyrrhenian Sea near the mouth. The flow directions are

closely related to the structural conditioning of the main alpine structural setting and are linked to the opening of the Tyrrhenian basin [6,7] (Figure 1).

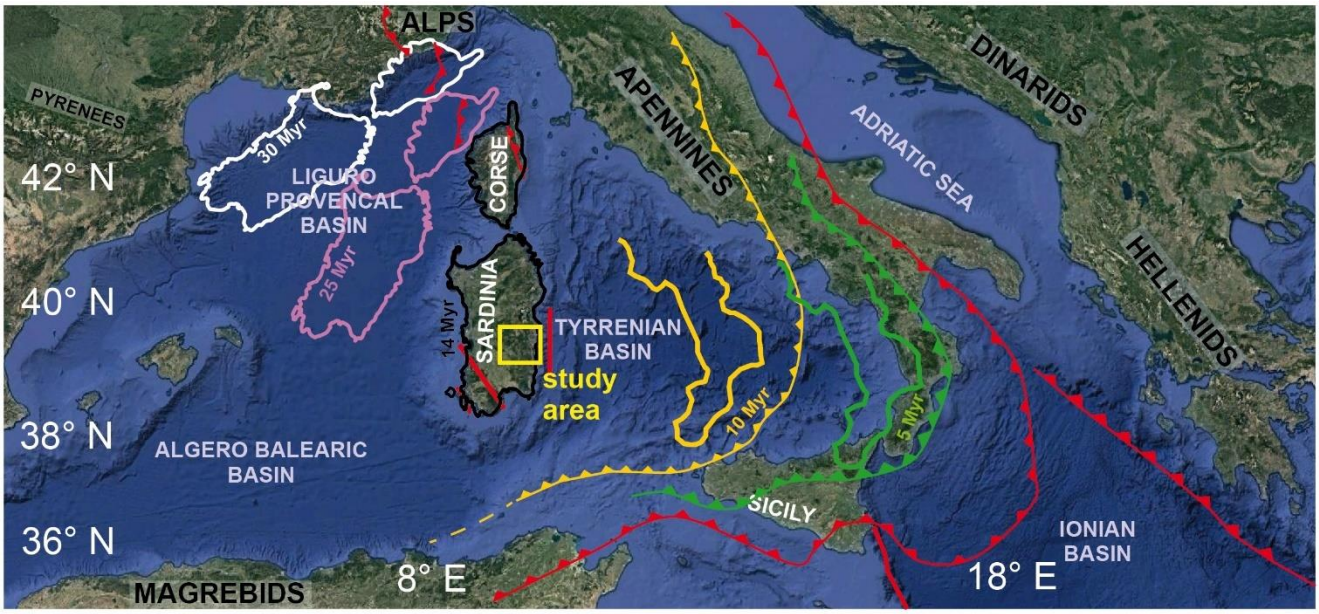


**Figure 1.** Geographical location and structural features of the study area, modified after [8]; red lines represent thrust fronts; white lines are the Sardinian–Corse Block translation at 30 Ma; the pink line represents the Sardinian–Corse Block translation at 25 Ma; the yellow line represents the Calabrian block translation at 10 Ma; the green line represents the Calabrian block translation at 5 Ma [2].

River drainage systems are very dynamic features of the landscape. Geological changes can cause fluvial captures, leading to abnormal large-scale river networks [7,9–16]. The main geological changes that cause river captures are glaciation and tectonic movements associated with earthquakes and faults [17]. Tectonic movements, especially landscape uplift, are much slower than glacial processes. Therefore, the development of tectonic river capture normally requires hundreds of thousands of years, or even millions of years [18,19].

The particular evolutionary characteristics of the Pardu and Quirra valleys in relation to slope instability dynamics have been the subject of various studies [4–7]. This sector of Sardinia represents one of the most susceptible areas to landslides in the region. This high hazard is closely linked to the particular vulnerability to important weather events, especially rainstorms. Rainfall-induced landslides represent a relevant threat to the population, infrastructure, buildings, and cultural heritage [20–24]. Among the most important catastrophic geological events in Sardinia are those that occurred in the Rio Pardu valley, which involved the inhabited centers of Gairo, Osini, Ulassai, and Jerzu. Between 15 and 17 October, 1951, extreme rainfall of about 1000 mm involved this area, triggering mudflows and landslides. This catastrophic event caused abandonment of the villages of Osini and Gairo [5,7,25]. These settlements have been rebuilt at least in part, sometimes with transfer to another area on the same slope. However, these measures proved useless, as the new sites present the same geo-hydrological risks as the previous ones [26,27]. Landslides affected schistose Paleozoic metamorphites on the left slope, while on the right, there was also widespread rockfall. Recent studies have highlighted the presence of deep-seated gravitational slope deformations with sacking [28–32] and lateral spread [33–35] characteristics that affect the sub-horizontal carbonate succession and the underlying metamorphites [6].

Deep-seated gravitational slope deformation (DGSD, [36]) is a complex type of rock slope failure characterized by large dimensions generated in stone rocks [37]. DGSDs are characterized by slow movements that can suddenly accelerate and cause catastrophic

collapse of sections of the deformed slopes [30,38–41]. Therefore, this phenomenon represents an important geo-hazard in relation to the deformation of large infrastructures and secondary collateral landslides. Although DGSDs play an important role in slope evolution and geo-hydrological risk, knowledge about them was scarce for a long time [42]. They are characterized by very slow deformation rates [34], landform assemblages (such as double-crested ridges, trenches, synthetic and antithetic scarps, tension cracks, and convex bulged toes), and deep basal shear zones [43–47]. Often, shear zones present characteristics of cataclastic breccias with an abundant fine matrix [48] and thicknesses up to tens of meters [41]. DGSD is a common phenomenon in the relief of the Mediterranean Sea in relation to the particular geodynamic context that characterizes the region and to the widespread orogenetic chains. In this context, DGSDs play an important role in slope relief evolution, showing at least geometric analogies with gravity-accommodated structural wedges. Often, DGSD phenomena are influenced by the scale structural context of the slope and use pre-existing tectonic structures (fault and thrust) to guide their evolution, which is also in relation to a reactivation linked to a slope stress field variation [49,50].

In Sardinia, the studies and evidence of DGSDs are quite scarce, but the distensive tectonics and the Plio-Quaternary uplift could justify the favorable conditions for the development of DGSDs, which could also be due to local reactivation of Hercynian and Alpine tectonic structures. In this context, the slope evolutionary characteristics are analyzed—in particular, the DGSDs and the evolution of watercourses in relation to the uplift. The aim is to correlate these different aspects through geomorphological analysis with both field surveys and remote sensing techniques. Furthermore, the choice to analyze these basins takes on a particular characteristic due to the economic and social repercussions that the conditions of instability of the slopes determine in the populations of the towns of Ulassai, Osini, Jerzu, and Gairo. In fact, as is well known, these inhabited centers are continually threatened by disasters. Different types of interventions were carried out to protect inhabited centers and infrastructures, but they were carried out without a global study of the problem and, therefore, without real knowledge of the evolutionary modalities of the valley and the real gravitational dynamics of the slopes. Understanding the kinematics and temporal behavior of DGSDs and landslides is important for designing monitoring systems based on strong process knowledge. In some cases, continuous monitoring is the only way to reduce risk [51–55].

We hypothesize that the Plio-Quaternary tectonics and uplift in the Ogliastra area are the main forcing mechanisms for sustaining the necessary gravitational forces of DGSDs.

Here, we present an innovative approach for analysis of DGSDs and fluvial dynamics by using morphotectonic, morphostratigraphic, and geomorphic data and time-series InSAR data in the Pardu and Quirra rivers. We also integrated stratigraphic and morphotectonic data of the drainage basin scale to support our observations and analyses about the relation between DGSD activity and fluvial capture.

## 2. Geological Setting

East-central Sardinia (Italy) is characterized by widespread Jurassic dolomitic plateaus—called "Tacchi" in Sardinia—overlying a Paleozoic basement (Figures 2 and 3a,b) [56,57].

The area is characterized by the Pardu River Valley in the north, the Quirra River Valley in the south, and the Rio Pelau toward the east (Figure 2). The geological basement primarily comprises low-grade Paleozoic metamorphites affected by complex plicative structures, while in the coastal sector, there are widespread outcrops of carboniferous granites placed in the terminal phases of the Hercynian orogeny [1,59–61]. The major metamorphic Paleozoic units are the Filladi del Gennargentu Formation and Monte Santa Vittoria Formation, which are constituted by metasandstones, quartzites, phyllites, and metavolcanites (Middle Cambrian–Middle Ordovician) [57,62,63]. The summit of the metamorphic basement has suffered chemical alteration associated with a warm humid climate during the Permian and Triassic periods [64,65].

The marine and transitional Mesozoic sedimentary succession rests on the metamorphic basement in angular unconformity. These Mesozoic deposits are extensive and decipherable from their plateau morphology and are clearly visible along the right slope of the Rio Pardu and the Rio Quirra (Figure 2). The basal layers are primarily fluvial sediments of the Genna Selole Formation (Middle Jurassic) (Figure 3d), which are overlain by dolomitic limestones of the Dorgali Formation (Middle–Upper Jurassic) (Figure 3e). [57,64,66,67].

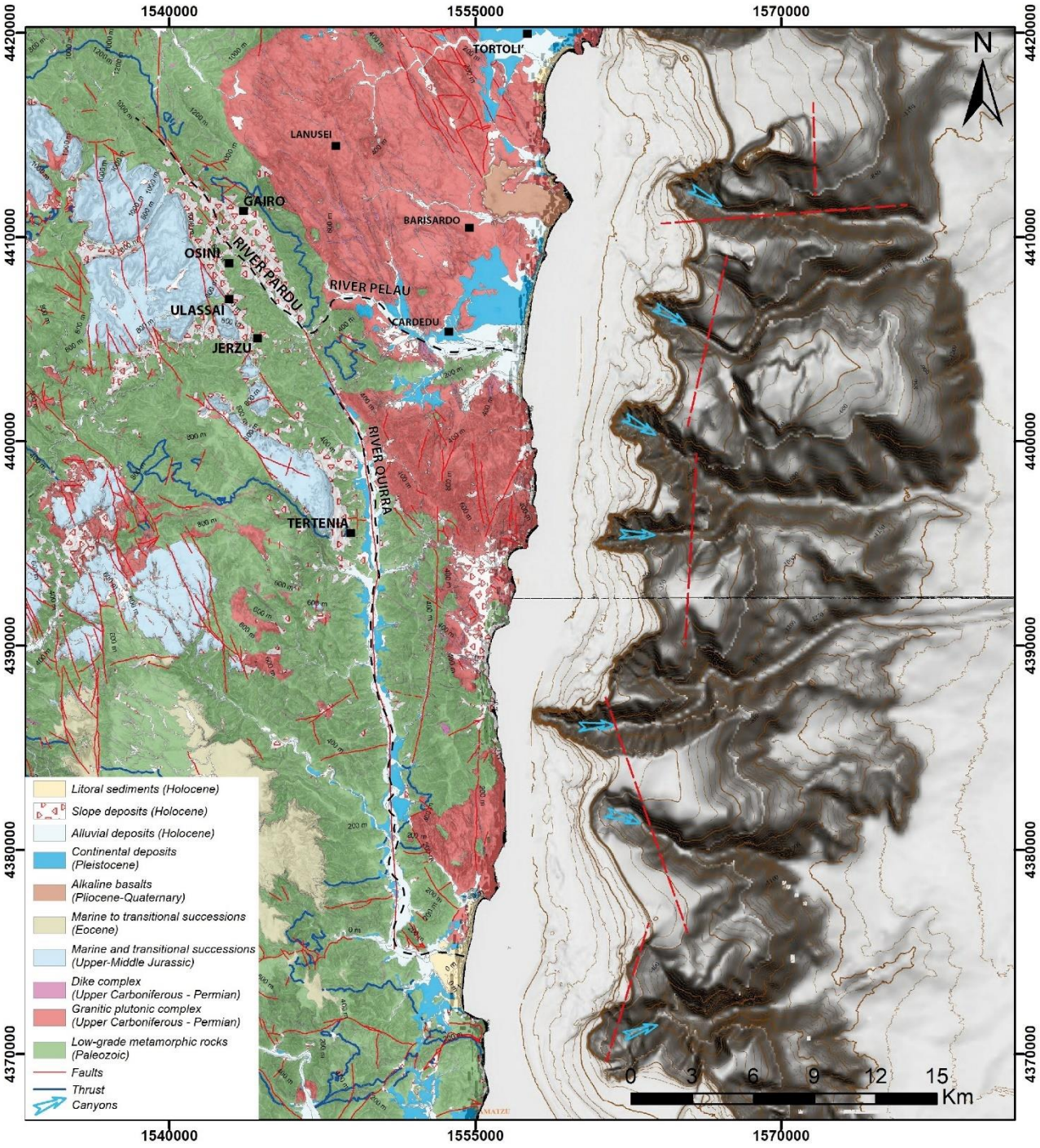


**Figure 2.** Geolithological sketch map of the study area based on geological data of the Autonomous Region of Sardinia. Continental margin topography by [58]. Black dashed lines show the analyzed rivers.

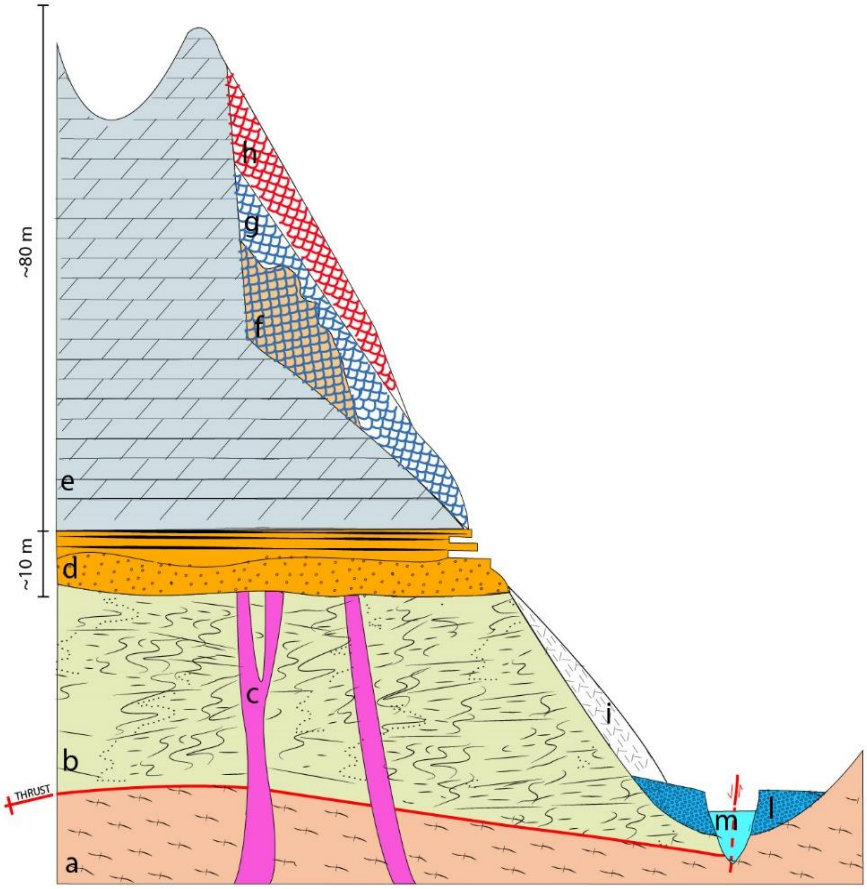


**Figure 3.** Lithostratigraphic sketch of lithological units: Low-grade metamorphic rocks: (a) Monte Santa Vittoria Fm; (b) Filladi del Gennargentu Formation; (c) granitic plutonic complex and dikes; marine and transitional Mesozoic sedimentary succession; (d) gluvial and deltaic conglomerates, sandstones, and mudstones (Genna SeloleFormation); (e) dolostone (Dorgali Formation); (f) cemented paleo-rockfall deposits; (g) paleo-rockfall deposits; (h) active rockfall; (i) slope deposits; (l) terraced alluvial deposits; (m) alluvial deposits (modified after Demurtas et al. [6]).

The Genna Selole Formation [67,68] represents a mixed succession of siliciclastic to siliciclastic–carbonate deposits. The presence of clay layers is important as a predisposing factor for lateral spread. The Dorgali Formation is represented by dolomitic sequences with thicknesses of up to tens of meters. The lower part, with a thickness of approximately 30 m, is affected by marl intercalations, whereas the upper part is typically massive. The attitude of the strata of the Mesozoic units is sub-horizontal with a dip of approximately N90/0–5°, while at the plateau edges, it can reach a dip of up to 40° and a direction parallel to the slope owing to the DGSDs. Quaternary covers, which are represented by continental deposits, are primarily gravitative and alluvial deposits. The most extensive outcrops are represented by landslide deposits, including rockfalls, toppling, and collapsed DGSDs, and are abundant in the lower part on the right slopes of the Pardu Valley and Quirra Valley (eastern slope of Monte Arbu). Downslope, actual and terraced alluvial deposits have also been identified, and they are well developed and hierarchized in the Rio Quirra [57].

The deposits of the rockfalls and toppling landslides have been characterized by their different sedimentological features based on age (Figure 3f–h). These deposits are associated with rockfalls affecting the plateau edge wall and the collapse of some parts of the DGSDs [6].

## 3. Geodynamic Setting

The river networks' geometry and gravity processes show a young conformation of the landscape, which is typical of a recent tectonic setting. The geodynamic setting is associated with the collisional dynamics between the African and European plates [2] (Figure 1). The structural setting is associated with the Alpine cycle, which first appeared with a strike-slip fault in the Oligo–Miocene, and then in the Pliocene and Quaternary with an extensional component [1–3,56,69–72].

The major features in the study area are the NW–SE and N–S faults on which, respectively, the Pardu Valley and Quirra River are engraved, and the secondary fault directions include ENE–WSW and NNE–SSW [57].

The Plio-Quaternary tectonic phase is associated with conspicuous N–S faults [73]. These rectilinear and normal faults are also evident in the continental margin and control its morphology (Figure 2). In the continental region, these N–S faults are associated with alkaline basalts with an age of approximately 3.9 Ma—Pleistocene [74]. Especially during the upper Pliocene, a general areal elevation occurred throughout the island, highlighted by the traces of the paleo-surfaces and by the numerous and superimposed paleo-hydrographies; moreover, the Neogenic sediments, which were already affected by Oligo-Miocene Tectonics, are currently also found at altitudes of 700 m, such as on the Tacco di Laconi, and are widely found above 500 m of altitude in various locations on the island. The reasons for these events are related to the more general distensive tectonics that affect the whole Tyrrhenian area [75].

Based on preliminary geodetic data from the Peri-Tyrrhenian Geodetic Array network, Ferranti et al. (2008) [76] revealed the presence of low internal deformation in Sardinia. In Sardinia, seismicity is typically scattered and sporadic, except for the dozen tremors detected following the ML4.7 earthquake of 7 July 2011 in the Corsican Sea, which primarily characterized the edges of the continental lithosphere block. Significant seismic events also occurred in the eastern sector—in particular, three events with a magnitude > 4 (26 April 2000, magnitudes ML 4.2 and 4.7, and 18 December 2004, magnitude ML 4.3)—located in the central Tyrrhenian Sea, approximately 60 km east of Olbia in the Comino depression [77].The most recent low-magnitude earthquake events were ML 1.8 (Escalaplano, 4 April 2019) and ML 1.6 (Perdasdefogu, 14 October 2020) [78].

Along the Ogliastra coast, recent movements have acted by conditioning the trend of the hydrographic network and the morphological evolution. The basaltic plateau of the Teccu in Barisardo can be related to these movements along an N–S line.

The Sardinian continental margin started from around 9 Ma, following the opening of the Tyrrhenian Sea, which caused the thinning of the continental crust and the formation of tectonic depressions, which are now sites of deep intra-slope basins.

The continental margin off the Ogliastra is represented by the continental shelf, the continental slope, and the plain called the Ogliastra basin, which reaches the deepest point of the whole Sardinian margin at 1750 m depth. The continental shelf is very narrow with less than 10 km of width, and it is indented by several submarine canyons [58,70].

## 4. Geomorphological Setting

The landscape, which is characterized by sub-horizontal carbonate plateaus, represents the result of the paleogeographic evolution of the region. The current dolomitic plateaus represent the extensive carbonate sedimentation due to the Jurassic marine transgression on the peneplanated Paleozoic metamorphites during the Permian and the Triassic. The continental phase following the post-Mesozoic emergence determined the setting of a tectonic control hydrographic network represented by deep rectilinear valleys engraved in the Paleozoic basement for several hundreds of meters [4,5] (Figure 4). Erosion primarily acted on the Oligo-Miocene strike-slip faults with an increase in the erosive rate during the Plio-Pleistocene uplift phases [25]. The presence of major regional faults has influenced the watercourses, which maintain a prevalent N–S direction in the Pardu and Quirra Rivers (set on the main fault).

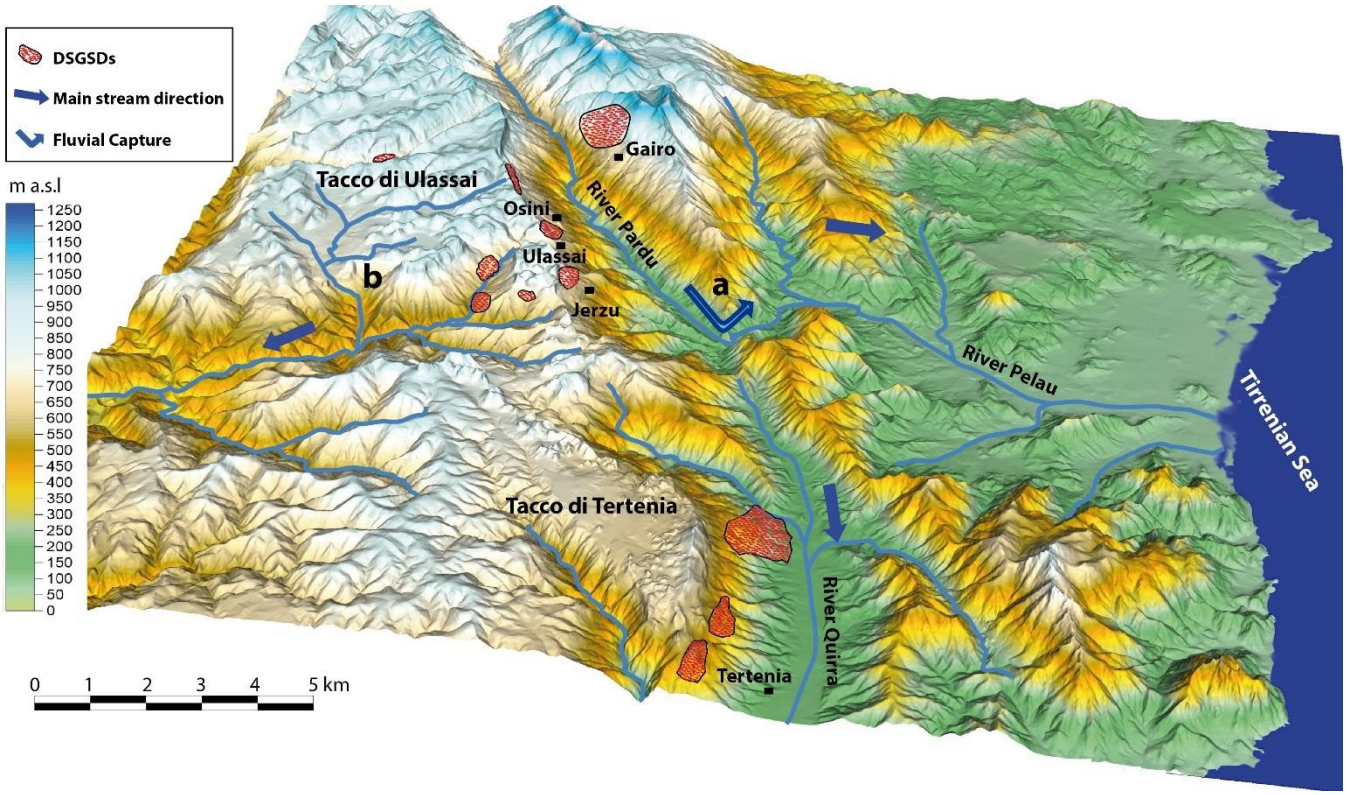


**Figure 4.** Three-dimensional (3D) model of the Pardu River and Quirra River. Blue lines represent major hydrographic features, and red areas represent the major DGSDs. (a) Fluvial capture elbow; (b) Lequarci waterfall.

The evolution of the Pardu River is closely associated with that of the Quirra River [7,57,79]. The Pardu River flows from the NW toward the SE and then abruptly changes direction toward the NE. At this point, a capture elbow adjacent to the present head of the Quirra River is well developed. The upstream part of the Quirra River flows at an altitude of approximately 200 m higher than the Pardu River. It also presents an over-sized and over-flooded valley with respect to the upstream catchment area. Moreover, there are various orders of river terraces and slope deposits of the Pleistocene. This setting indicates that the Pardu River, previously flowing south along the Quirra River, was captured by the Pelau River [7,79]. Considering the descriptive parameters, longitudinal profile, and the evolutionary conditions, the Pardu Valley is associated with a cycle of underdeveloped fluvial erosion, suggesting a relatively young age of engraving [4,5,25].

DGSDs are present in both river basins and cause collateral landslides. In particular, rockfalls and toppling occur along carbonate cornices, while rotational slide occurs in the metamorphic rocks [6]. We focused on the DGSDs in this study, as they are important in the morphological evolution of the slopes.

A significant karstic process has acted on plateau surfaces, comprising ancient paleo-forms and, currently, hypogeal and superficial morphologies [6,7,80]. Karst paleoforms represented by complex cockpit doline types have been characterized, and they belong in a humid and warm paleo-morphoclimatic setting [6,81–83]. These dolines are separated by residual reliefs called Fengcong, which are sorted among the major structural features. The hypogean karst enabled the development of sinkholes, karst springs, cavities, and caves (e.g., Su Marmuri Cave and Is lianas Cave). The combined action of karst, uplift, river erosion, and gravity has led to the formation and evolution of hanging valleys on the plateau surfaces [5]. The geomorphological analysis of the continental margin off the coast shows that the area occupied by the shelf is rather narrow and is engraved with numerous submarine canyons [58,84,85] (Figure 2). The structural lines coincide with those of the continental part that has emerged—mainly N–S, accompanied by normal tectonic lines in

the E–W direction. The shelf break is about −130 m; however, locally, it is at about −60 m due to the erosion of retrogressive canyons. The submerged and emerged morphologies highlight the extremely young landscape conformation, which is associated with the Neogene and Quaternary geodynamic events, implying a series of problems related to the slope process. The control factors of the DGSDs are associated with the geo-structural characteristics and the Neogene and Quaternary geomorphological evolution of the river valley, which is associated with the recent uplift [6].

We can summarize the events that dominated the valleys' evolution [4,6,79]:

- The first stage preceding the capture of the Rio Pardu by the Rio Pelau associated with the uplift and the Plio-Quaternary tectonics. This phase involves a general incision of the valleys and erosion of the slopes, and it led to a new hydrographic setting, causing river capture (Middle-Lower Pleistocene).
- The second phase was associated with major erosive activity in the Pardu Valley following the capture, which led to complete erosion of the valley (Upper Pleistocene).
- The present evolution of the slopes through widespread landslides and DGSDs.

## 5. Materials and Methods

A morphotectonic analysis of the River Pardu and River Quirra was carried out based on an integrated approach that incorporated a cartographic and morphometric analysis [86–88]. Remote sensing analysis and geological and geomorphological field mapping in slopes and the valley floor of the Rio Quirra and Rio Pardu were performed from the head to the mouth on a scale of 1:10,000. The field surveys were based on the interpretation of data from remote sensing on a large scale. Particular attention was paid to the study of morphologies related to river dynamics (fluvial and orographic terraces) and slope gravitational process (DGSDs and collateral landslides).

Multi-scale field surveys were carried out to analyze the geological and structural setting of the slopes—in particular, the plateaus' edges and the left slope of the Pardu Valley [89–94].

The DGSDs were surveyed in detail by reconstructing the structural setting and analyzing the relationships with the surrounding collateral landslide and alluvial deposits. The study areas were often not accessible due to their steep slopes; therefore, they required remote sensing survey systems to complete the field investigations. Uncrewed aerial vehicle digital photogrammetry (UAV-DP) is a robust methodology for the investigation of DGSDs and large landslides. In particular, it was used for the recognition of large lateral spreads in Malta and Tunisia [95,96]. We used UAV-DF and light detection and ranging (LiDAR) to extract high-resolution topographic 3D DGSD models and perform detailed morphometric analyses.

DGSD displacement and rate were evaluated using space-borne interferometric synthetic aperture radar (InSAR). Over the last 30 years, InSAR techniques have been widely used to investigate geological (e.g., volcano activity, earthquakes' ground effects, etc.) and geomorphological processes—in particular, DGSD. In different geological and climatic contexts, this technique allows one to analyze extremely slow DGSDs and to identify displacements of about 1–2 mm in favorable conditions [95–103].

Based on previous studies on the fluvial deposits of Rio Quirra and Rio Pardu [5,6,79], the geological analysis was implemented by using high-resolution topographies based on UAV-DP and LiDAR. Detail-scale field surveys were carried out in the alluvial quaternary deposits with the aim of the identification and mapping of various terraced orders and the reconstruction of the relative chronology among morphostratigraphy and sedimentological indicators. Stratigraphic profiles relating to the various orders of river terraces and landslide deposits were surveyed in the natural outcrops of the alluvial plains.

### *5.1. Aerial and Uncrewed Aerial Vehicle Remote Sensing*

LiDAR and aerial photogrammetric data produced by the Autonomous Region of Sardinia were used to perform visual and morphometric analysis of DGSDs and fluvial

morphologies. A detailed orthophoto dating from 2016 was used together with LiDAR data with a cell size of 1 × 1 m and vertical resolution of 30 cm.

The aerial surveys were performed using UAVs (DJI Phantom 4 and DJI Matrix 200) flying at altitudes of 50–60 m above ground level. The acquired images were analyzed and processed using the photogrammetric Agisoft MetaShape software and constrained by 10–12 ground control points using GEODETIC LEICA GNSS for each area. The resulting orthorectified mosaic and DEM (WGS 84 datum and UTM 32N projection) had a cell size of 5 cm/pixel and were considered sufficiently precise to be used for the geomorphological analysis.

To analyze the DGSDs at the local scale, we used high-resolution digital elevation models (DEMs) acquired via structure from motion from a UAV-DF [8,103–106].

The 3D high-resolution UAV-DF models were used to develop interpretative superficial models by using geomorphological evidence and stratigraphic and structural data of the DGSDs. Geological interpretative cross-sections of geologic features crossing the major DGSDs were also generated to define the movement kinematics, deformative style, and deep geometries of the DGSDs.

The DTMs were used to analyze the morphometric parameters of the hydrographic basins under analysis. The longitudinal and transversal profiles of the valleys were extracted in such a way as to highlight different erosive structures in relation to river capture and to analyze the different altitudes of the various river terraces.

### *5.2. InSAR Analysis*

Space-borne interferometric synthetic aperture radar (InSAR) data were used to analyze the slope deformation [107–110]. Interferometric permanent scatters (PSs) are used to investigate the temporal and spatial superficial slope deformation. To detect ground displacement, we used only high-PS coherence (0.6–1) located on built dolomitic blocks and the metamorphic rock outcrops. Low-coherence PSs, which are not useful, are located on rockfall deposits and in vegetated areas. We used the Sentinel-1 and European Remote Sensing (ERS) satellites (Table 1) and took into account the line-of-sight (LOS) velocities. We used a dataset from 1992 to 2000 from the ERS satellite and a dataset from 2014 to 2020 from Sentinel 1. The processed data from ERS and Sentinel 1 were provided, respectively, by Ministero dell'Ambiente e della Tutela del Territorio e del Mare (Italy) and the Geological Survey of Norway. The total area analyzed covered the entire Pardu Valley and Quirra Valley. Four focus areas (Table 1) that showed interesting results were analyzed by using time series of PSs to understand the landslides' temporal evolution.

**Table 1.** Parameters of the InSAR data on the sectors in focus.

| Area | Satellite | Acquisition Geometry | Acquisition Interval | TrackAngle | Inc Angle |
|---|---|---|---|---|---|
| Ulassai | Sentinel 1 | Ascending | Oct 2014–Feb 2020 | −9.6 | 42.4 |
| Osini | Sentinel 1 | Ascending | Oct 2014–Feb 2020 | −9.6 | 42.4 |
| San Giorgio | Sentinel 1 | Ascending | Oct 2014–Feb 2020 | −9.6 | 42.4 |
| Gairo | Sentinel 1 | Descending | Oct 2014–Feb 2020 | −169.6 | 36.3 |
| | ERS | | May 1992–Dec 2000 | - - - - - | - - - - - |

## 6. Results

### *6.1. InSAR, PS, and Time Series Analysis*

The results of the large-scale InSAR analysis showed that most PSs were located in stable areas, while high deformation rates were recorded in the slopes of Pardu Valley, where slope-failure processes—in particular, rockfalls and DGSDs—were widespread. All four focus areas were analyzed in detail with the Sentinel 1 data (from 2014 to 2020). For the left flank of Rio Pardu, the ERS data (from 1992 to 2000) were also used in descending order of acquisition. The data from the periods 1992–2000 and 2014–2020 indicated areas with large slopes that were identified as DGSDs that were active in Pardu Valley. We used

only PSs with high coherence (0.6–1) that were located in the rocky outcrops and in the urban structures, while low-coherence points located in rockfall deposits and in vegetated areas were not considered. The PS analysis allowed the recognition of active DGSDs and the measurement of their movement rates, which turned out to be extremely slow, ranging from 6 to 20 mm/year (Figures 5 and 6). We identified a downslope movement of up to 1 cm/y in the right slope of the Pardu Valley and a movement of up to 2 cm/y in the left slope. Continuous movements that did not change over years with both linear and seasonal trends were observed (Figure 6). The InSAR analysis showed no perceptible movements on the slopes of Rio Quirra.

In the Ulassai area, the PS analyses showed a stable surface in the urban area and on the west slope of the main extensional trench of Pranedda Canyon (Figures 5a and 6a). However, in accordance with the geomorphological evidence, downstream from the main trench, the speeds of the PSs showed LOS displacements of up to 1 mm/y. In this sector, the PSs were located in rocky dolomitic outcrops on the top edge of the plateau, in the total absence of vegetation and in excellent exposure conditions. No movements were detected in the DGSD downstream from Bruncu Pranedda due to the low PS coherence due to dense vegetation. Using Sentinel data from 2014 to 2020, we measured a total of 5 cm (orange star in Figure 5). It was possible to observe seasonal deformation trends with an excellent correlation among all of the PSs analyzed. Generally, no movement was observed during the winter and spring, but an acceleration was observed during the summer and autumn.

In Osini, a cluster of PSs were well defined within the inhabited center, particularly in the northwest and southeast sectors, where there was a speed of between 4 and 6 mm/y, with a maximum of 8 mm/y (Figures 5c and 6b) with a seasonal trend. Spotlights were located on the roofs of the buildings. In the surroundings of the inhabited center, the dense vegetation resulted in a low coherence of the PSs; therefore, they were not considered.

In the Gairo sector, the InSAR data showed a large area that was greater than 1 $km^2$ with a high diffusion of PSs. Based on the high-resolution field surveys, the PSs are located on rocky metamorphic outcrops. The speeds were, on average, greater than 8 mm/y, with a maximum of 2 cm/y. The cluster identified a well-defined area with a circular shape that was delimited by PSs with zero or negligible speed (Figures 5b and 6d1,d2). The higher speeds were located in the central and basal part of the DGSD, while towards the top and lateral flanks, the speeds decreased. In the lateral and top parts, the DGSD was delimited by stable PSs (speeds of 0–2 mm/y), which allowed the deformed area to be circumscribed in detail. in the PSs on the foot slope with a low coherence due to the continuous movement of slope deposits and the vegetation were not considered. The deformation's progression was continuous and linear, and an excellent correlation was found between the Sentinel 1 and ERS data. In the southern part of the DGSD, a high concentration of PSs were located in the abandoned village of Old Gairo with speeds that were sometimes greater than 1 cm/y. The town of New Gairo, which was built after the 1951 catastrophe, showed displacements limited to 2–4 mm/y.

In the San Giorgio sector, scattered PSs were identified with speeds greater than 10 mm/y on the large blocks of the rock avalanche on the slope (Figures 5d and 6c). These blocks, with dimensions of up to 30 m per side, were collateral landslides related to the collapsed DGSD located at the edge of the plateau above. All of the PSs showed a linear trend with a slowdown in the winter and spring between 2016 and 2017. This slowdown, which was observed in all of the PSs, indicates that the causes of the movement are to be found in processes that involve a greater portion of the slope, and not only in the large blocks. The surrounding area did not allow a PS analysis due to the importance of the wooded vegetation, but evidence of deformation was visible in the road infrastructure.

### *6.2. Deep-Seated Gravitational Slope Deformation*

Various areas affected by DGSDs and landslides that were located of the slopes of Pardu Valley and on the slope of Monte Arbu of Tertenia were identified (Table 2).

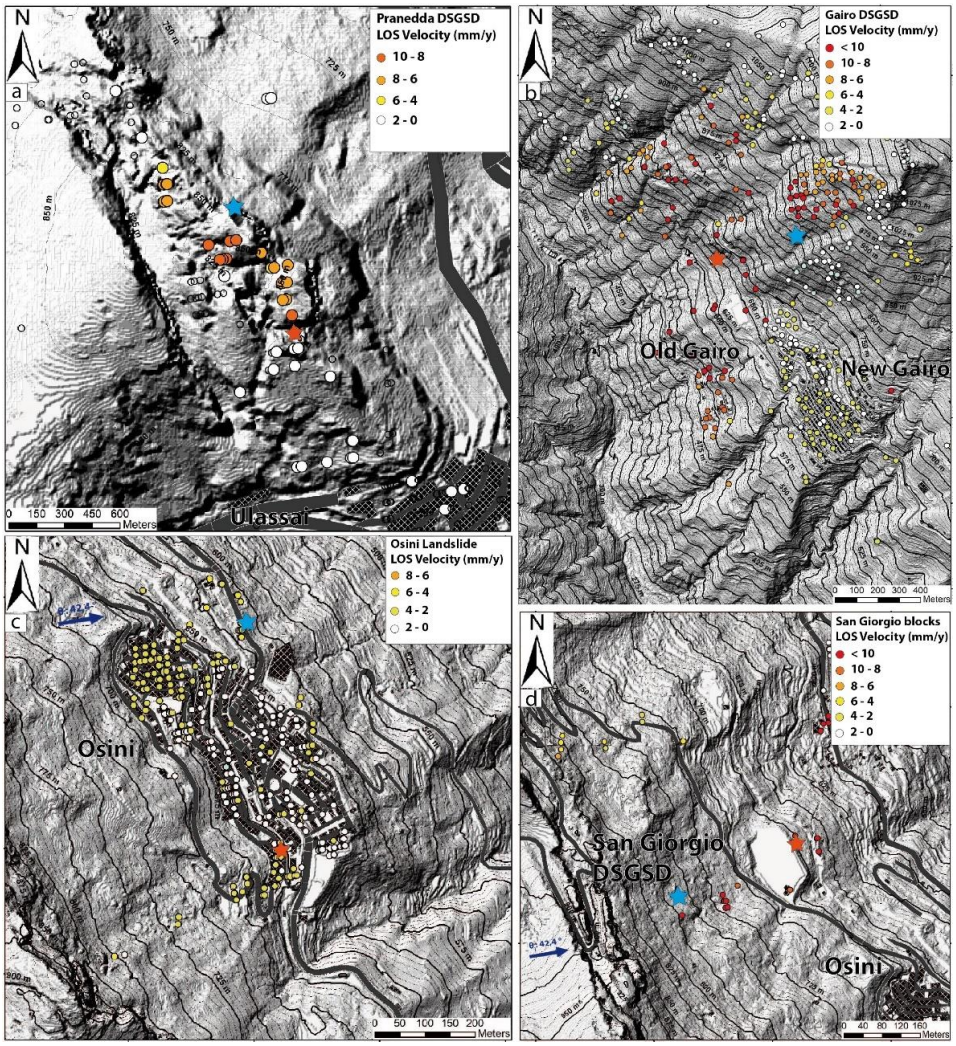


**Figure 5.** Analysis of the focus areas with InSAR data. The points represent high-coherence permanent scatters located on buildings, rocky outcrops, and blocks of large rock avalanches. The stars represent the PSs used to analyze the time series shown in Figure 6. (**a**) Bruncu Pranedda lateral spread. (**b**) Gairo DGSD. (**c**) Osini landslide. (**d**) San Giorgio paleo-rock avalanche.

On the east side of Tacco di Ulassai and Tisiddu Mountain, three DGSDs were analyzed (Figure 7). The main structures that indicated deep gravitational phenomena were large and deep extensional trenches that were evident in the dolomitic lithotypes. The extensional trenches had lengths of several hundreds of meters and a decametric opening and depth. This slope was characterized by the Mesozoic marine deposits resting on the Paleozoic metamorphites.

The Bruncu Pranedda DGSD (Figure 7b2,c1) is constituted by two regions with different settings located on the top and middle slopes. On the top slope, toward the east of the largest extensional trenches in the area called the Pranedda Canyon, the rock mass fracturing increased, and the attitude of the Dorgali Formation was toward the east, with a dip of up to 40°. In this area, both facies of the Dorgali Formation were visible, with the summit comprising dolomitic banks and the lower part being characterized by an alternation of well-stratified dolomites and marls. This subdivision was not observed in the middle slope, where basal marly levels did not appear on the surface. This indicates that the basal facies (approximately 30 m) were partially covered by slope deposits; however, they also sank a few meters inside the fractured and altered Paleozoic metamorphic basement. This could be correlated with the field observations at the same altitude, as well as with the basement and the massive facies of the Dorgali Formation [6].

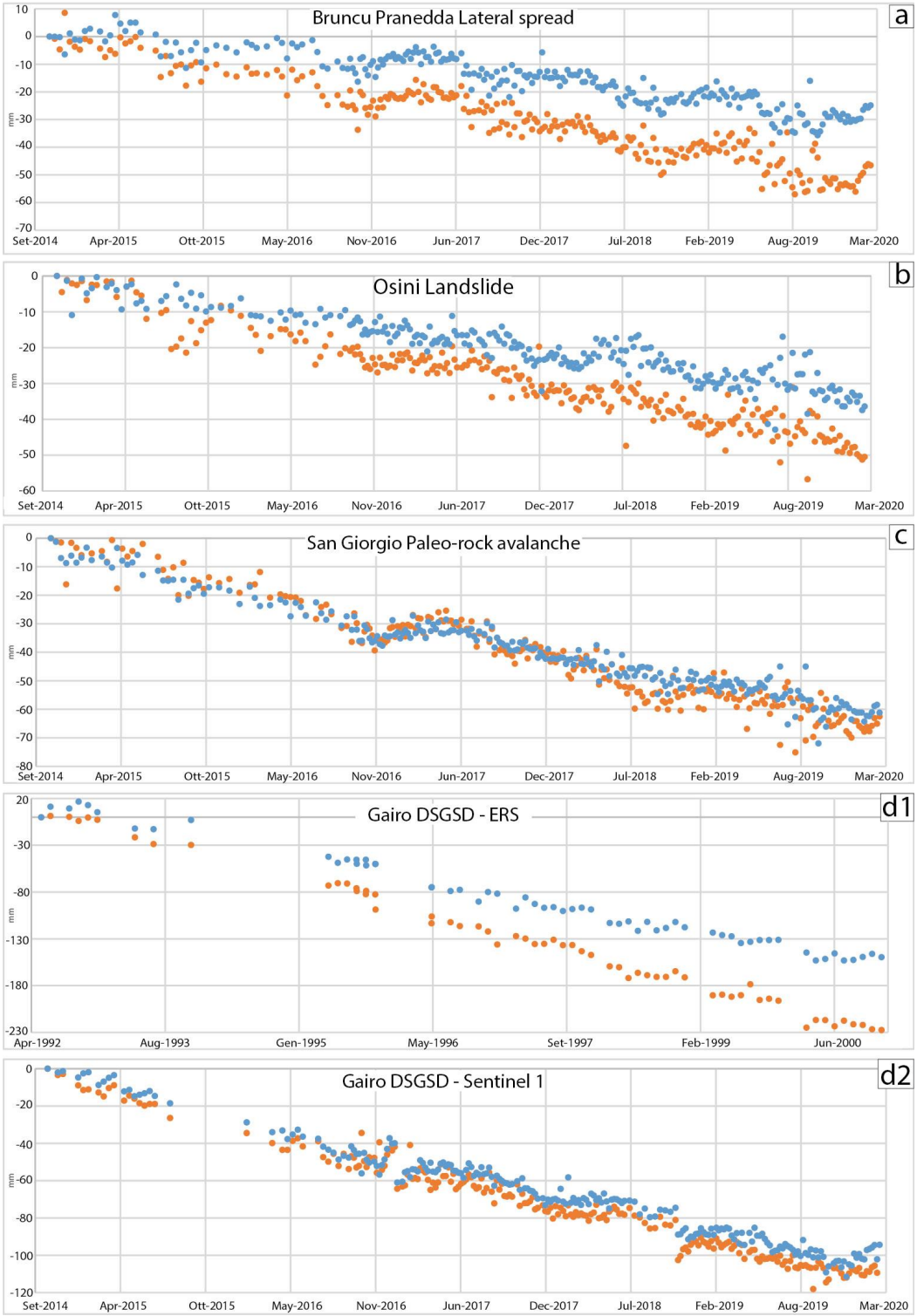


**Figure 6.** Time series extracted with the representative permanent scatters. The vertical axes represent the cumulative LOS displacement; the horizontal axes represent the time. (**a**) Bruncu Pranedda lateral spread—seasonal displacement trend, maximum displacement of 5 cm from 2014 to 2020; (**b**) Osini landslide—seasonal displacement trend, maximum displacement of 6 cm from 2014 to 2020; (**c**) San Giorgio paleo-rock avalanche—constant movement trend of the large blocks, maximum displacement of 6 cm from 2014 to 2020; (**d**) Gairo DGSD; (**d1**) the ERS data show a constant deformation trend, with a maximum displacement o f23 cm from 1992 to 2000; (**d2**) the Sentinel 1 data show a constant deformation trend that is correlated with the ERS data, with a maximum displacement of 10 cm from 2014 to 2020. The colors of the points agree with the colors of the stars that identifies the location of the PS in Figure 5.

**Table 2.** Main characteristics of the DGSDs and landslides analyzed.

| Location | Landslide | Geology | Landslide Kinematic | Displacement Speed mm/y | Displacement Trend | Area $Km^2$ |
|---|---|---|---|---|---|---|
| North Ulassai | Bruncu Pranedda Lateral spread | Dolomitic limestone set on altered and fractured phillites | Lateral spread top slope; sackung middle slope | 6–10 mm/y | Seasonal | 0.2 |
| South Ulassai | Monte Tisiddu Sackung | Dolomitic limestone set on altered and fractured phillites | Sackung | No movement | —— | 0.2 |
| North Osini (San Giorgio) | San Giorgio Lateral spread | Dolomitic limestone set on altered and fractured phillites | Lateral spread | No movement | —— | 0.03 |
| North Osini | San Giorgio paleo-rock avalanche | Megablock rock avalanche deposits set on paleo-rockfalls | Sliding | 6–>10 | Linear | ≈0.1 |
| Osini | Osini Landslide | Cemented paleo-rockfalls set on phillites | Sliding | 4–8 | Seasonal | ≈0.3 |
| Gairo | Gairo DGSD | Phillites on metavolcanites. Slope involved in Hercinical thrust | Sackung | 6–20 | Linear | 1.2 |
| South Tertenia | Tertenia DGSD | Dolomitic limestone set on altered and fractured phillites. Slope involved in Hercinical thrust | Sackung | No movement | —— | 1.5 |
| North Tertenia | Paleo-DGSD | Dolomitic limestone set on altered and fractured phillites | Sackung | No movement Fossilized by Pleistocenic alluvium | —— | 1.5 |

The Scala San Giorgio DGSD (Figure 7b1,c2,d1) is located north of Osini Village and is characterized by two major extensional trenches that are parallel to the slope affecting the Dorgali Formation with a dip amount of up to 20°. All of the sequences of the Dorgali Formation are exposed; however, the Genna Selole Formation is covered by rockfall deposits.

The Tisiddu Mountain DGSD (Figure 7b3,d2) to the south of Ulassai Village is characterized by a highly fractured segment of the Dorgali Formation located tens of meters downstream. Only the tops of the massive banks of dolostones are visible. The basal level partially sank into the metamorphic basement.

In all cases, the shear zones are located in different geological units that represent structural weaknesses (Figure 7d1,d2). (I) The top of the metamorphites was affected by sub-horizontal foliation and advanced weathering, which was highlighted by the reddish or whitish color of the rocks. This type of alteration could be linked to the pre-transgressive Mesozoic period [65]. (II) The Genna Selole Formation was characterized by plastic clay layers; (III) basal levels of the Dorgali Formation were characterized by the alternation of marl and dolomite.

A large landslide that affected the town of Osini and the northernmost slope downstream of the San Giorgio DGSD was identified by using InSAR data. The inhabited center of Osini is built over an extensive cemented paleo-rockfall deposit that rests on the Paleozoic basement. Geomorphological evidence is difficult to observe due to the extensive vegetation around the village.

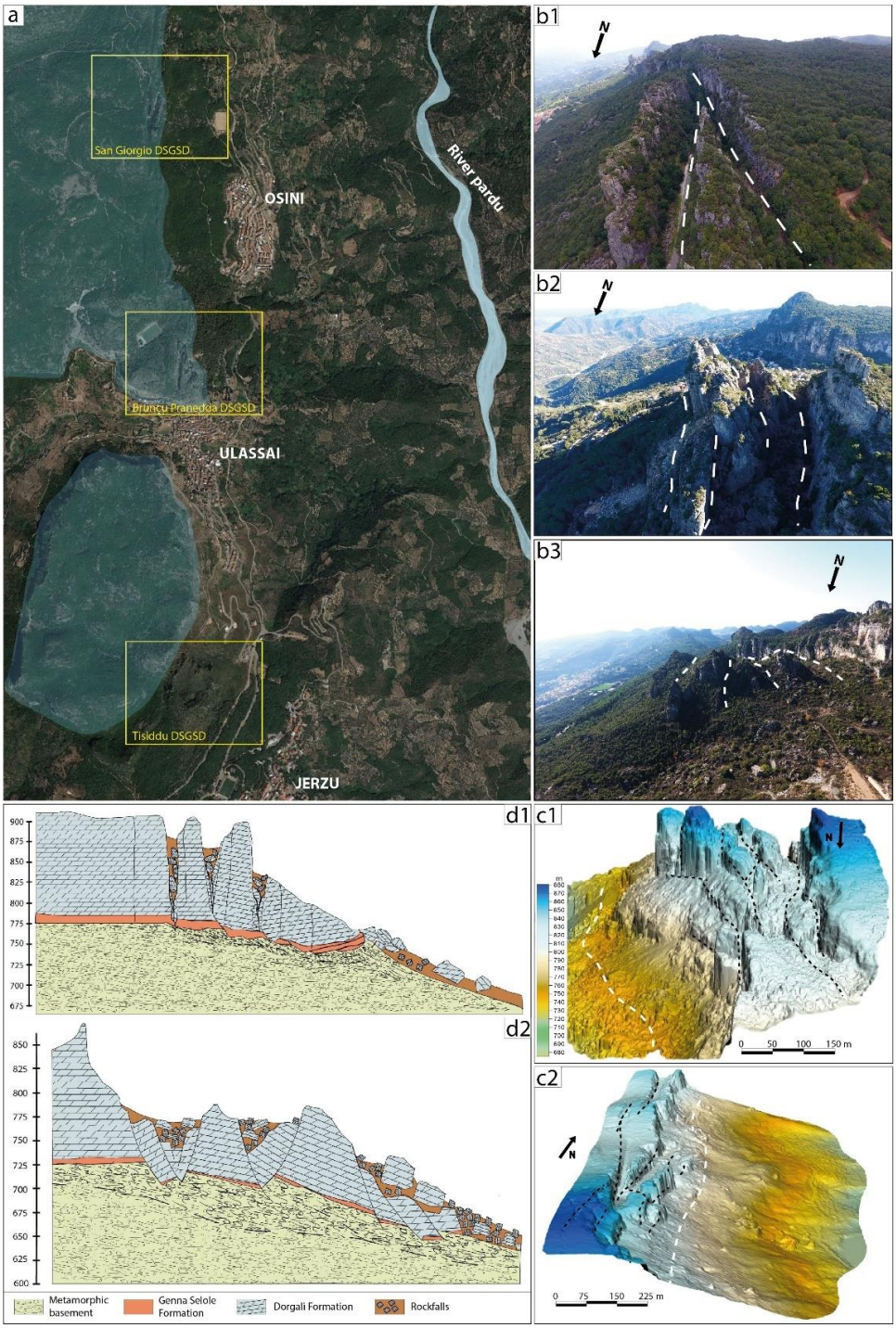


**Figure 7.** DGSD on the right slope of the Pardu River. (**a**) Orthophoto of the area of Ulassai, Osini, and Jerzu. The Jurassic dolostone plateaus on the metamorphic basement are shown in blue. The yellow square represents the analyzed DGSD. (**b**) UAV images of the DGSD showing the major geomorphological and structural features. The white dashed lines represent the major extensional trenches. (**b1**) San Giorgio lateral spread, (**b2**) Bruncu Pranedda lateral spread, (**b3**) Monte Tisiddu sackung. (**c**) Three-dimensional LiDAR model of the DGSDs with a colored elevation scale. The black dashed lines represent the major extensional trenches. The white dashed lines represent the major stratigraphic discontinuity between the marine Mesozoic sequence and the metamorphic basement. (**c1**) Bruncu Pranedda lateral spread. (**c2**) San Giorgio lateral spread. (**d**) Interpretative geological cross-sections passing through the DGSD in the study area. The hypothetical basal shear zone is highlighted with black dotted lines. (**d1**) San Giorgio lateral spread. (**d2**) Monte Tisiddu sackung.

The left side of the Rio Pardu is characterized by a different geological and structural context compared to the opposite side (Figure 8a). There are metamorphic lithologies belonging to the formation of Monte Santa Vittoria and the Filladi del Gennargentu. The slope is affected by a dip-slope Hercynian thrust that brings the two formations belonging to two different tectonic units into contact. This structure plays a fundamental role in the deep gravitational processes, as it is marked by intense fracturing and alteration of the lithotypes. Based on the geomorphological evidence and the analysis of the InSAR data, a large landslide with a DGSD character was identified in the northwest sector with respect to the town of Gairo (Figure 8b–f). The DGSD extends from the top slope to the middle-lower part of the slope and is about 1 km wide. The crown is circular (Figure 8c,d) and joins laterally rectilinear structural flanks (Figure 8e). Analyzing the profile of the slope along the DGSD, the concave upstream part and the convex downstream part are clearly evident. The foot of the landslide is covered by landslide and slope deposits that reach the valley floor, where lateral erosion by the Rio Pardu is affected (Figure 8).

On the right side of the Rio Quirra, in correspondence with the Tacco di Tertenia, complex gravitational morphologies linked to paleo-DGSDs are evident (Figure 9). The morphology of Mount Arbu is also affected by the complex tectonic structure, which is characterized by a sub-horizontal thrust that brings the Pyllades del Gennargentu Formation into contact with the Metavolcanites of the Monte Santa Vittoria Formation (Figure 9a). The morphological analysis of the slope shows convexity and concavity linked to different DGSDs that are distributed at various altitudes of the slope. The DGSDs consist of portions of the Dorgali Formation, which is tilted up to 30–40° and is translated along the slope. The most complex and evolved movement was identified in the NE sector (Figure 9b,c1,c2). The area extends for a length of about 1800 m from the top of the plateau to the valley floor. The fan-shaped landslide body has a foot with a length of 2 km. The crown is located in the plateau edge, which is affected by faults and distension trenches. The latter delimit mega-blocks of the Dorgali Formation With a prismatic shape and inclination of up to 40°. The foot of the DGSD, which is represented by the Dorgali Formation, is marked by dolomitic outcrops with vertical heights of up to 40 m with sometimes sub-horizontal attitudes of the strata. On these walls, terraced alluvial deposits rest in onlap. Paleo-DGSDs are widespread in the upper part of the slope, with greater diffusion in the southern part of Mount Arbu, but they do not evolve until reaching the valley floor (Figure 9b,d).

### *6.3. River Capture Analysis*

The area has a deep cut made by the Rio Pardu Valley and Rio Quirra Valley, which extend in an NNW–SSE direction, following a major Tertiary fault. For most of the Pardu River's course, the talweg is set on rock, indicating its predominantly erosive nature. Downstream, the river is captured, turning in an eastward direction, and its name changes to Rio Pelau; then, it flows into the Tyrrhenian Sea. South of the capture, the abandoned Rio Pardu Valley continues southward as Rio Quirra. This valley is characterized by a bottom filled with Pleistocene and Holocene terraced alluvial deposits and slope deposits, which are currently undergoing erosion. It is clear that in the past, Rio Pardu was captured by Rio Pelau (Figure 10), causing a rapid incision upstream. Longitudinal profiles were constructed for Rio Pardu, Rio Quirra, and Rio Pelau. Rio Pardu flows up to 750 m below the dolostone near Ulassai, where the main active DGSDs are located. The evolutionary hypotheses are related to the Pliocene and Quaternary uplift, which led to an important erosive phase.

The triggering process can be justified in the following ways:

- An erosive increase caused by a generalized uplift that led to the retreat towards the inland by the head of the Rio Pelau until it connected with the Rio Pardu.
- Another hypothesis foresees the presence of a direct fault with an east–west course along which the Rio Pelau is set. In this case, the differential uplift of the block on which the Rio Quirra is currently set could justify the capture process as tectonogenic.

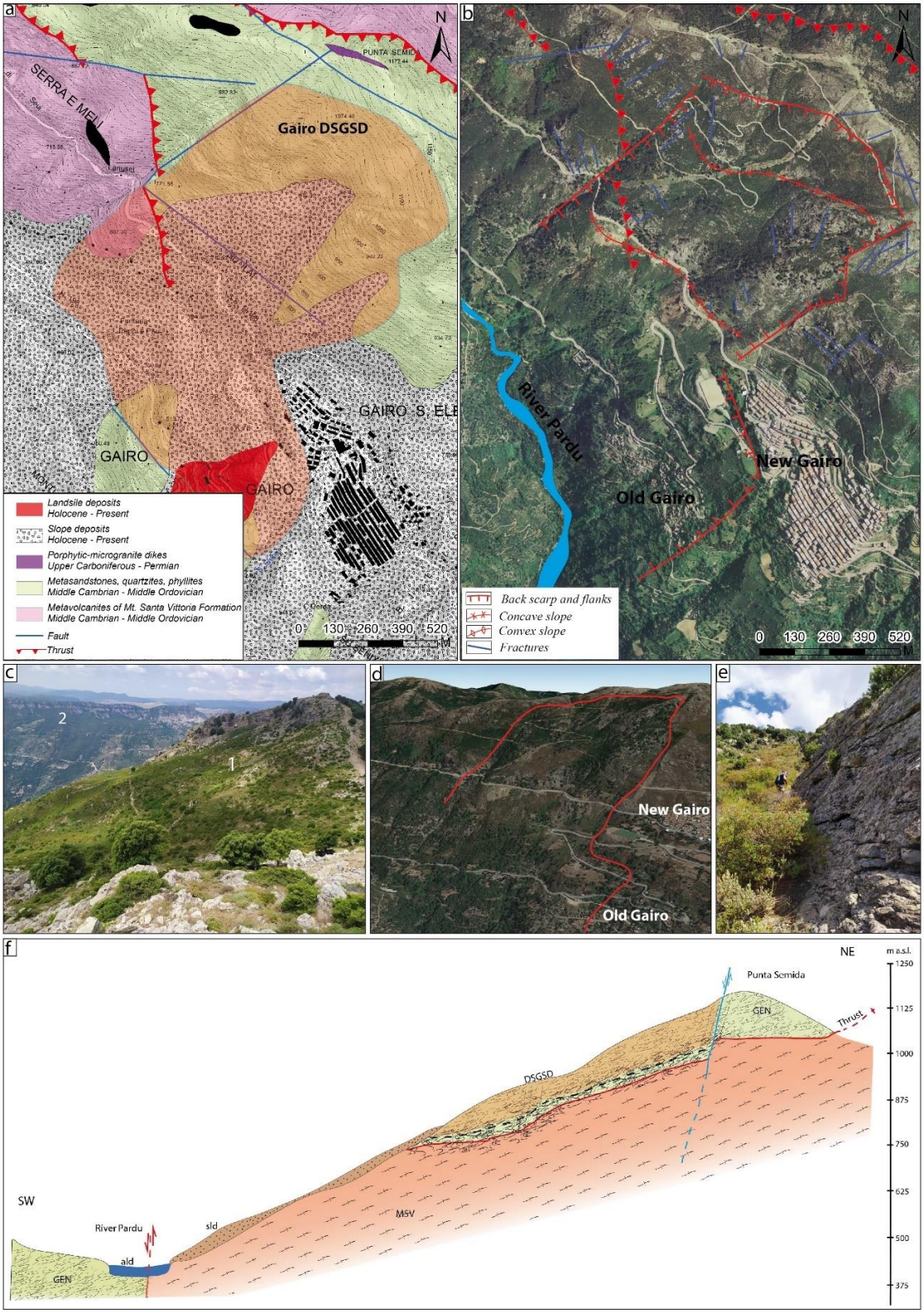


**Figure 8.** (**a**) Geological map of the Gairo slope with the DGSD localization. (**b**) Orthophoto with the main geomorphological feature of the DGSD. (**c**) Photo of the DGSD head. (1) Crown; (2) right slope of the Pardu River; (**d**) photo showing a 3D view with the DGSD border marked in red; (**e**) linear flank of the DGSD; (**f**) interpretative geological cross-section of the DGSD showing it (in transparent orange) sliding on the highly fractured rock due the underlying dip-slope Paleozoic thrust. Geolithological legend: MSV—Monte Santa Vittoria Formation; GEN—Filladi del Gennargentu Formation; ald—current alluvial deposits; sld—slope deposits.

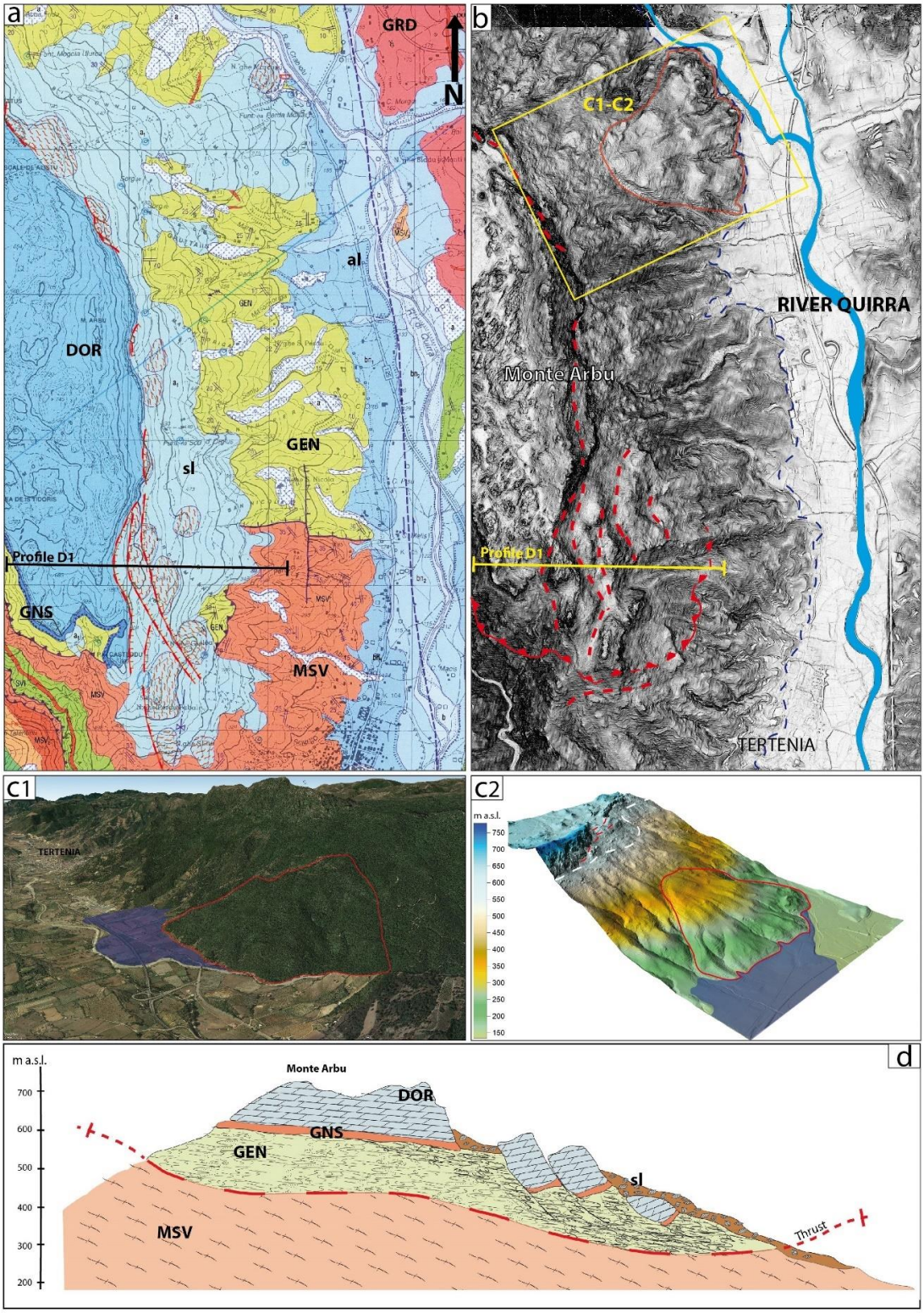


**Figure 9.** (**a**) Geological map of the eastern slope of Monte Arbu (Tertenia). Geolithological legend: MSV—Monte Santa Vittoria Formation; GEN—Filladi Del Gennargentu Formation; GNS—Genna Selole Formation; DOR—Dorgali Formation; al—terraced and current alluvial deposits; sl—slope deposits. [57]. (**b**) LiDAR hillshade with the main geomorphological feature of the DGSD. (**c1**) Photographic 3D view with the DGSD border marked in red and the terraced alluvial deposit in blue. (**c2**) Three-dimensional LiDAR of the Tertenia paleo-DGSD with the border marked in red and the terraced alluvial deposit in blue. (**d**) Interpretative geological cross-section of the DGSD showing it sliding on highly fractured rock due the underlying Paleozoic thrust.

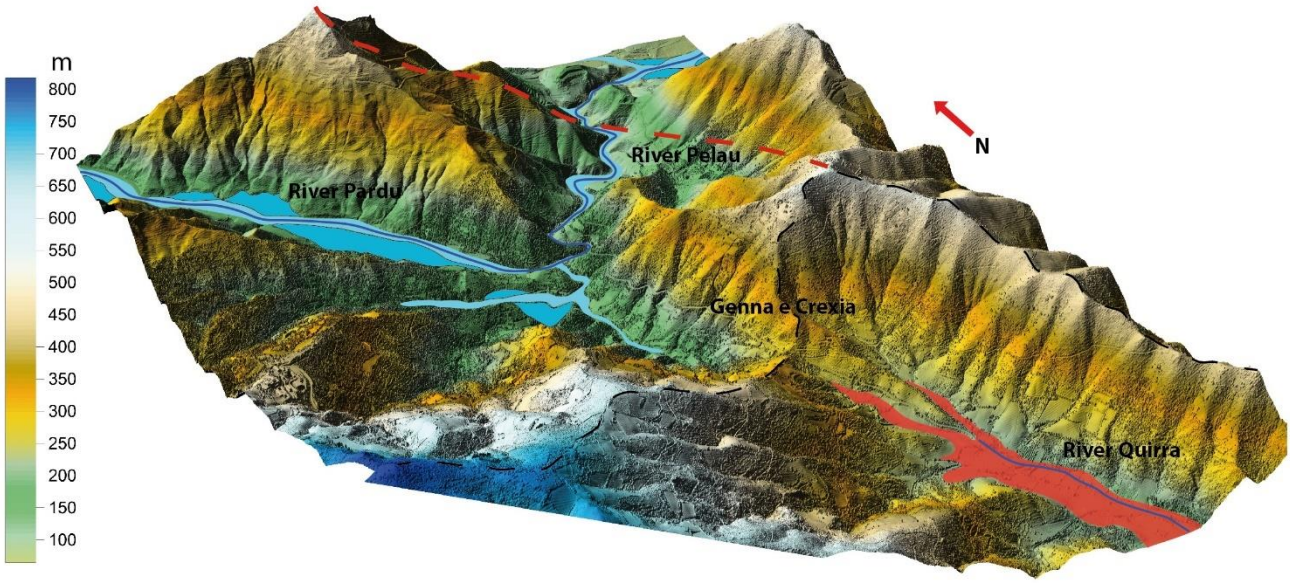


**Figure 10.** Three-dimensional LiDAR model of the river capture sector. In the north, the Pardu River flows eastwards, taking the name of Rio Pelau. The blue and light blue show the Holocene alluvial deposit of the Pardu River. South of Genna and Crexia is the head of the Rio Quirra. In red is shown the paleo-slope and paleo-alluvial deposits of the Quirra River.

### *6.4. Fluvial Morphostratigraphic Analysis*

A morphostratigraphic analysis was performed first on Rio Quirra and later on Rio Pardu, which isolated it following the capture (Table 3).

**Table 3.** Morphostratigraphic synthesis.

| Deposits | Characteristic | Elevation from Talweg | Distribution |
|---|---|---|---|
| T0 | Pebbles and clastosustained gravels with a scarce sandy matrix | 0 | Actual embrided riverbed |
| T1 | Heterometric and polygenic pebbles with a scarce dark matrix | 0.20/0.30–1.5 | Pardu-Quirra |
| T2 | The matrix is decidedly prevalent in the coarse fraction | 2–5/6 | Quirra |
| T3 | Non-constant matrix–skeleton relationship. Reddish matrix (Fe oxides) | 6/7–10 | Quirra |
| Paleo-conoid C1 | Clastosustained pebbles up to 40–50 cm in size. Scarce matrix | 30 | Pardu |
| Paleo-conoid C2 | Reddish pebbles and gravels in sandy, silty, reddish matrix | 15 | Quirra |
| Paleo-slope deposits | | 20–40 | Quirra |

In the valley of the Rio Quirra, above the current riverbed, the following were identified (Figure 11):

T0—Actual flood surface consisting of pebbles and clastosustained gravels with a scarce sandy matrix (Holocene).

T1—Sub-current Holocene terrace with a maximum height on the riverbed of about 20–30 cm up to 1.5–2 m. The dark brown matrix is subordinate to the coarse fraction, which is represented by heterometric and polygenic pebbles. This terrace often forms alluvial islands in the upstream part of the river; they reach a good stability due to the dense vegetation that has settled there (Upper Pleistocene–Holocene).

T2—In this terrace, the matrix, which is decidedly prevalent in the coarse fraction, has a dark brown color. There is no evidence of prolonged chemical alterations due

to climatic conditions other than the current ones. The pebbles are less varied: mainly quartz with, subordinately, granite and schistose. On average, the height of T1 with respect to the riverbed is about 2 m, with a maximum of 5–6 m and a minimum of 50 cm. The deposits that form this terrace show forms of erosion linked to secondary climatic pulsations (Upper Pleistocene).

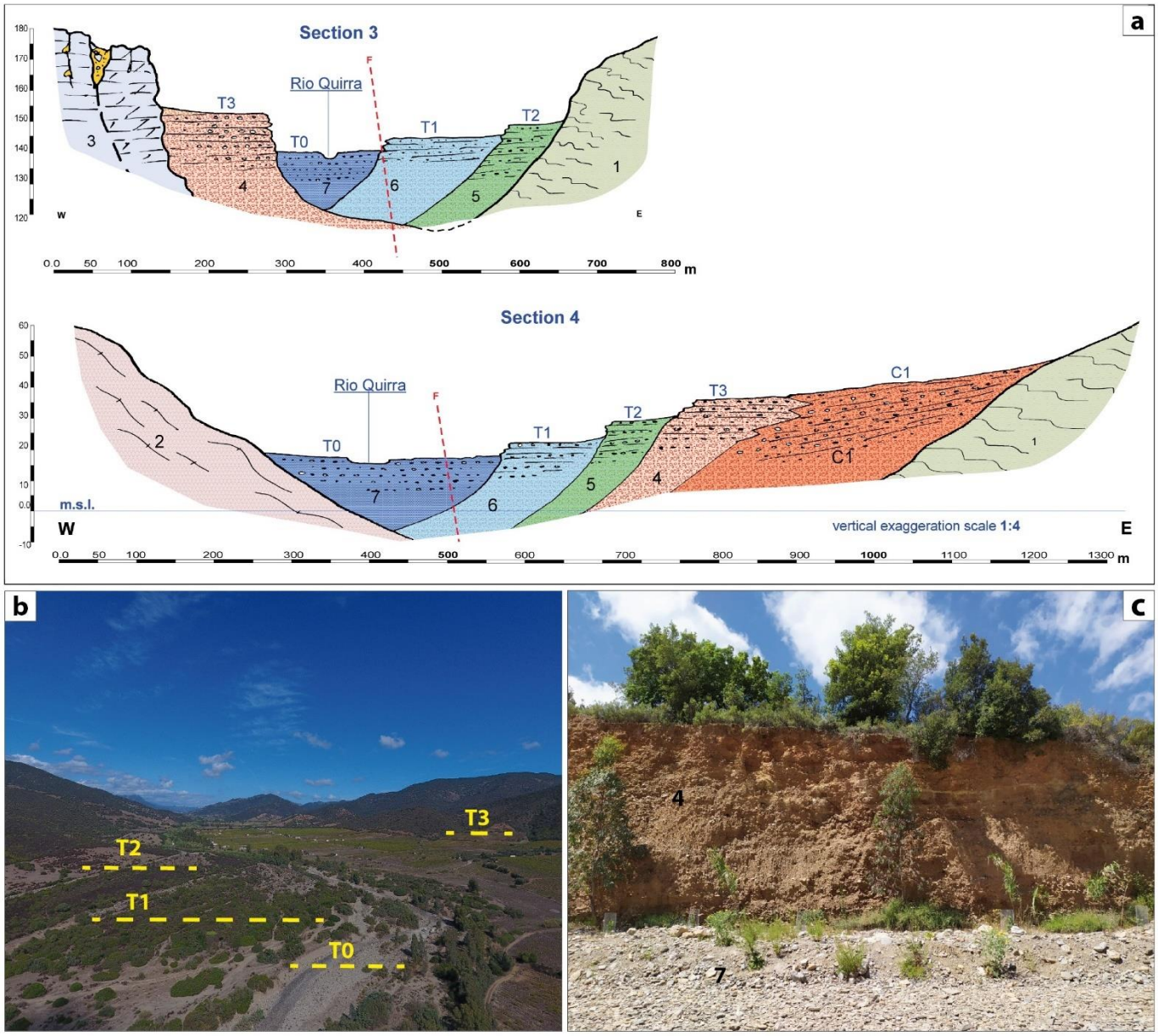


**Figure 11.** (**a**) Morphostratigraphic profiles of the Quirra River. (**b**) UAV photo in the river alluvial plain. (**c**) Outcrop of Terrace T3. Lithological legend: (1) Filladi Grigie del Gennargentu Formation; (2) Monte Santa Vittoria Formation; (3) paleo-DGSD; (C1) paleo-conoid; (4) T3; (5) T2; (6) T1; (7) T0.

T3—This is the oldest terrace, with an average height of 6–7 m and a maximum of 10 m (Figure 10c). The matrix–skeleton relationship is not constant. The depository is made up of alternations of fine and large sediments that testify to the variations in the river's energy. The matrix is red and sometimes whitish. In the first case, the color derives from Fe oxides, indicating a warm, humid climate typical of tropical and sub-tropical regions; in the second case, the oxides have been leached and for an eluviation horizon. The pebbly fraction does not have a varied lithological composition. It is mainly schistose

and, subordinately, quartz. The deposit is well cemented. This terrace rests directly on the slope. The frame of erosion along the riverbed is clear, and the lower terraces rest on it (Middle Pleistocene).

In Rio Pardu, the alluvial deposits cover a valley floor characterized by a well-defined flood bed, which is limited by banks that are intensely affected by landslides. Two orders of alluvial terraces up to 2 m above the current level were detected (Figure 12). The maturity of the flood clasts is very low due to the continuous supply of material from the slopes, while the grain size distribution along the longitudinal profile reflects the trend characterized by the high slope. By analyzing the longitudinal profile of the Rio Pardu, it can be observed that it is divided into two well-defined parts separated by the knickpoint in Ponti Mannu. In the initial part, near the steeply sloping trunk, there is the head of the valley, which continues until an area with a low slope where alluvial deposits appear. Downstream of the Ponte Mannu, after a section of the river in which the waters flow on the rock, the river becomes slightly sloped and establishes an alluvial plain with anastomotic channels and river islands.

Active and quiescent dejection cones are distributed over the Quirra and Pardu Valleys. The active conoids are well highlighted by the morphology, and they have a poorly elaborated clastic component and an uncemented dark brown matrix. In the terminal part of the Quirra, a terraced dejection cone (C1) assumes a certain importance due to its size and evolutionary stage (Inner–Middle Pleistocene). The often large pebbles are very elaborate and have blackish patinas of Mn oxides on their surfaces. Oxides also accumulate inside the matrix, which presents an intense redness. In the upper part of the Rio Pardu, a paleo-conoid (C2) with large pebbles and a brown matrix is currently engraved by the current course of the river (Upper Pleistocene and Holocene).

The paleo-slope deposits are characterized by coarse, elaborate, and sharp-edged components. The matrix is very abundant, strongly cemented, and bright red in color due to the accumulation of pockets of Mn oxides. These deposits are located at the same altitude as that of T3 or sometimes at higher altitudes, and they are connected to the base of the slope (Inner-Middle Pleistocene).

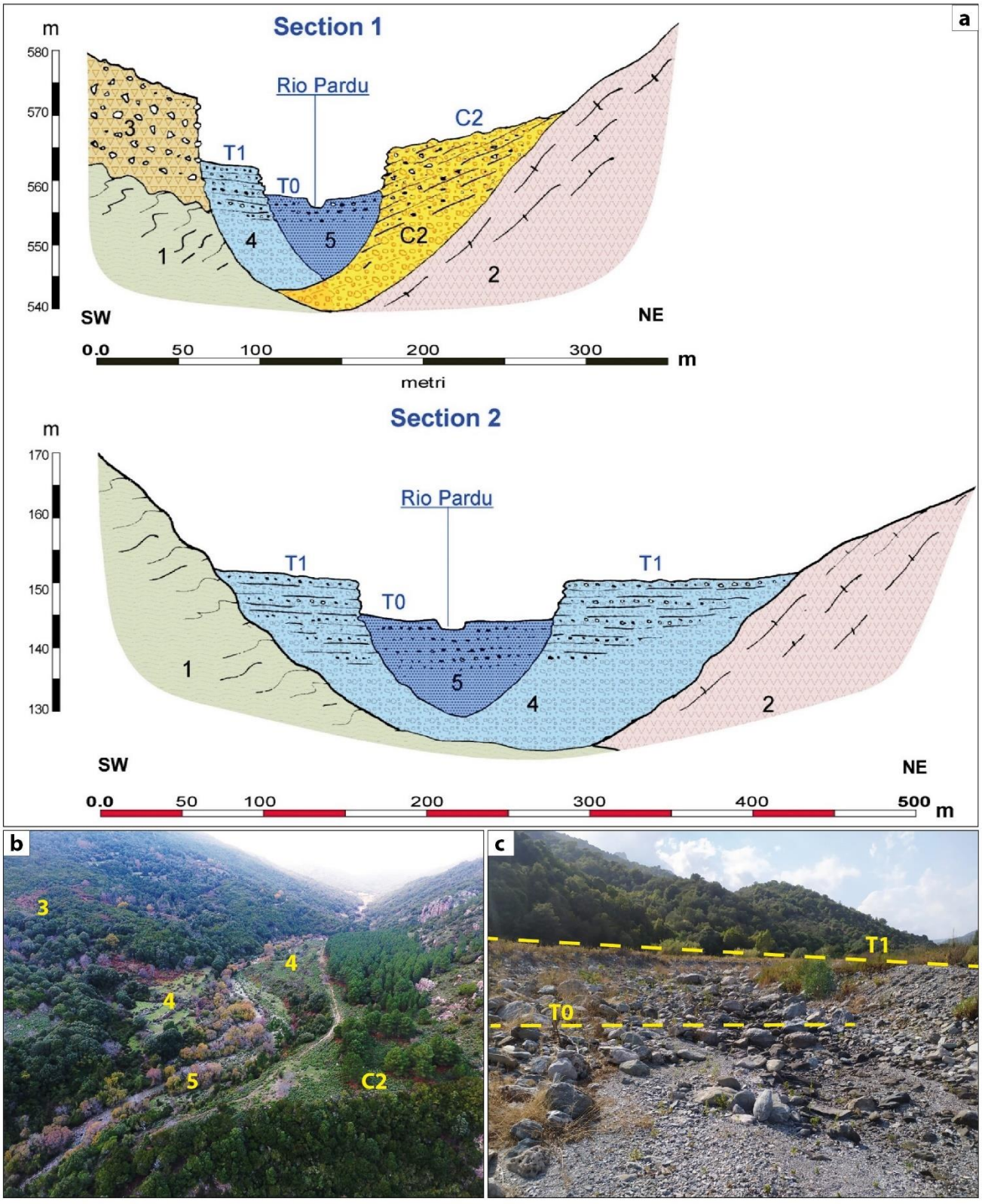


**Figure 12.** (**a**) Morphostratigraphic profiles of the Pardu River. (**b**) UAV photo near the head of the Pardu River. (**c**) The bottom of the Pardu Valley near the capture elbow. Lithological legend: (1) Filladi Grigie del Gennargentu Formation; (2) Monte Santa Vittoria Formation; (3) paleo-rockfall deposits; (C2) paleo-conoid; (4) Terrace T1; (5) Terrace T0.

## 7. Discussion

### *7.1. River Analysis*

The hydrographic network engraved by torrential watercourses possesses a tectonic control linked to the Cenozoic structural features. The main incisions that cross the basin of the Rio Pardu give rise to deep valleys with a mainly erosive and only locally depositional character. The Pardu Valley has a transverse "V" profile, which is more or less open depending on the evolutionary stage, the distance from the point of origin, and the competence of the lithotypes in which the river incision takes place. Sometimes, the profiles show marked asymmetries due to the different positions of the layers or the different exposure, which influences the vegetation. A lower steepness can be observed on the left side, which probably due to a lower vegetation cover, which favors erosion. The valley has developed in the formation of the Filladi grigie del Gennargentu. Only in the southeast is the formation of Monte Santa Vittoria affected.

As regards the evolutionary conditions of the Pardu Valley, considering the descriptive parameters, the geometric conditions, and the hypsometric curve, it is noted that was not able to develop to the point of acquiring characteristics that are attributable to a cycle of river erosion in an evolved phase, which suggests a relatively young age for engraving [4,5,25].

The longitudinal profile of the Rio Quirra differs from the normal profile of a river; it has an initial concave part with a strong steepness within the first kilometer from the head and a regular decrease in the slope along the rest of the watercourse. The evolutionary stage of the Quirra appears to have advanced; however, it must be considered that it represents the middle and final parts of the original Rio Pardu–Quirra, which are divided in two by the capture of the Rio Pelau. Currently, the Rio Quirra does not have a catchment basin at the head, and its feeding is mainly given by certain tributaries. The valley is oversized and over-flooded with respect to the current basin (Figure 13).

### *7.2. DGSD Dynamics*

The Rio Pardu and Quirra River represent two of the most susceptible areas to landslides in Sardinia, as well as to rockfalls and rainstorm-induced superficial landslides [4,5,26]. This sector is also interesting due to the fact that extreme rainfall over the last centuries has led to the evacuation and reconstruction of the towns of Osini and Gairo [5,7]. Recent studies have highlighted the presence of deep landslides with sackung-type kinematics and lateral spreads on the right side of the Rio Pardu [6].

In this paper, by analyzing integrated geomorphological, geo-structural, high-resolution topography and InSAR displacement data, we identified diffuse DGSDs on both sides of the valleys of the Pardu River and Quirra River, which are characterized by different kinematics.

DGSDs are commonly found in orogenetic environments with high tectonic and seismic activity and in areas affected by slope decompression due to post-deglaciation. The present work aimed to contribute to the knowledge on the influence of evolution of valleys—in particular, with high incision—on the triggering of large landslides or DGSDs in relation the Quaternary uplift.

Lateral spreads were developed at the edge of the plateau in relation to the favorable stratigraphy (dolostone on clays and altered metamorphites). The slope deformation generates vertical fractures in the carbonate and a zone of ductile basal deformation that affects the Genna Selole Formation and the summit, which thus altered the metamorphites (Bruncu Pranedda and San Giorgio DGSD). DGSDs with a higher vertical shift represent a more advanced stage with sackung features (Tisiddu Mountain and Tertenia DGSDs). The latter evolves in relation to the thrust that affects the median part of the slope. A large part of the deformation affects the Paleozoic basement, which was evidenced by the sinking of the carbonate sequence into the metamorphites.

On the left side of Rio Pardu, Gairo's DGSD shows a different behavior in relation to the different stratigraphic and structural setup. The DGSD has sackung-type kinematics with an important translational component linked to the thrust.

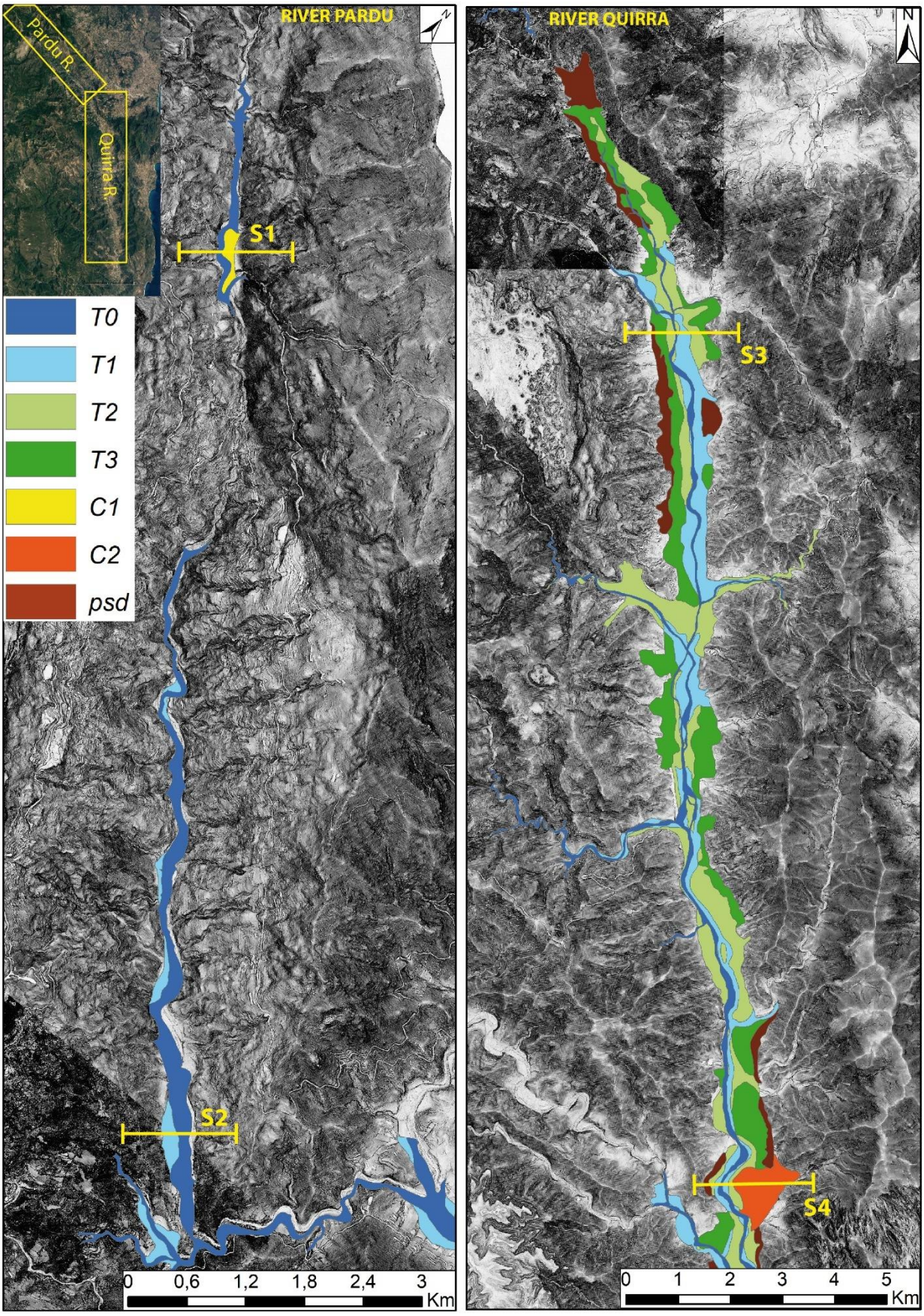


**Figure 13.** Map of the distribution of alluvial deposits in Rio Pardu and Rio Quirra.

From the structural viewpoint, the major faults in the NW–SE and NE–SW directions were in concordance with the main trenches and back-scarps in all sectors, indicating an important structural control. The secondary trenches and the joints did not exhibit a good correlation with the large-scale structures because they were associated with the features inside the deformation rock mass.

The Rio Pardu shows a straight valley with steep slopes, a valley bottom with a mainly erosive character, and two orders of terraces. This is linked to the intense erosive phase following the capture by the Rio Pelau. The valley of Rio Quirra shows a flat-bottomed valley with an actual riverbed of the braided channel type. The valley is over-sized and over-flooded with four orders of terraces, the result of an evolution prior to the capture of the Rio Pardu. The T3 terrace shows sedimentological characteristics related to a sub-tropical climate, which is probably linked to the warm climatic phase of MIS 5. The InSAR and morphostratigraphic analyses made it possible to define the state of activity of the DGSDs in the two hydrographic basins. In the valley of Rio Pardu, various areas of the slope that are affected by movements that can be classified as active DGSDs were identified, with movements of up to 2 cm/y on the left slope and up to 1 cm/y on the right slope. However, in the Quirra River, paleo-DGSD bodies are fossilized by the alluvial deposits of the T3 terrace. This indicates that the river capture led to an intense erosive phase in the Rio Pardu, leading to the recent instability of the slopes, thus justifying the active DGSD (Figure 14).

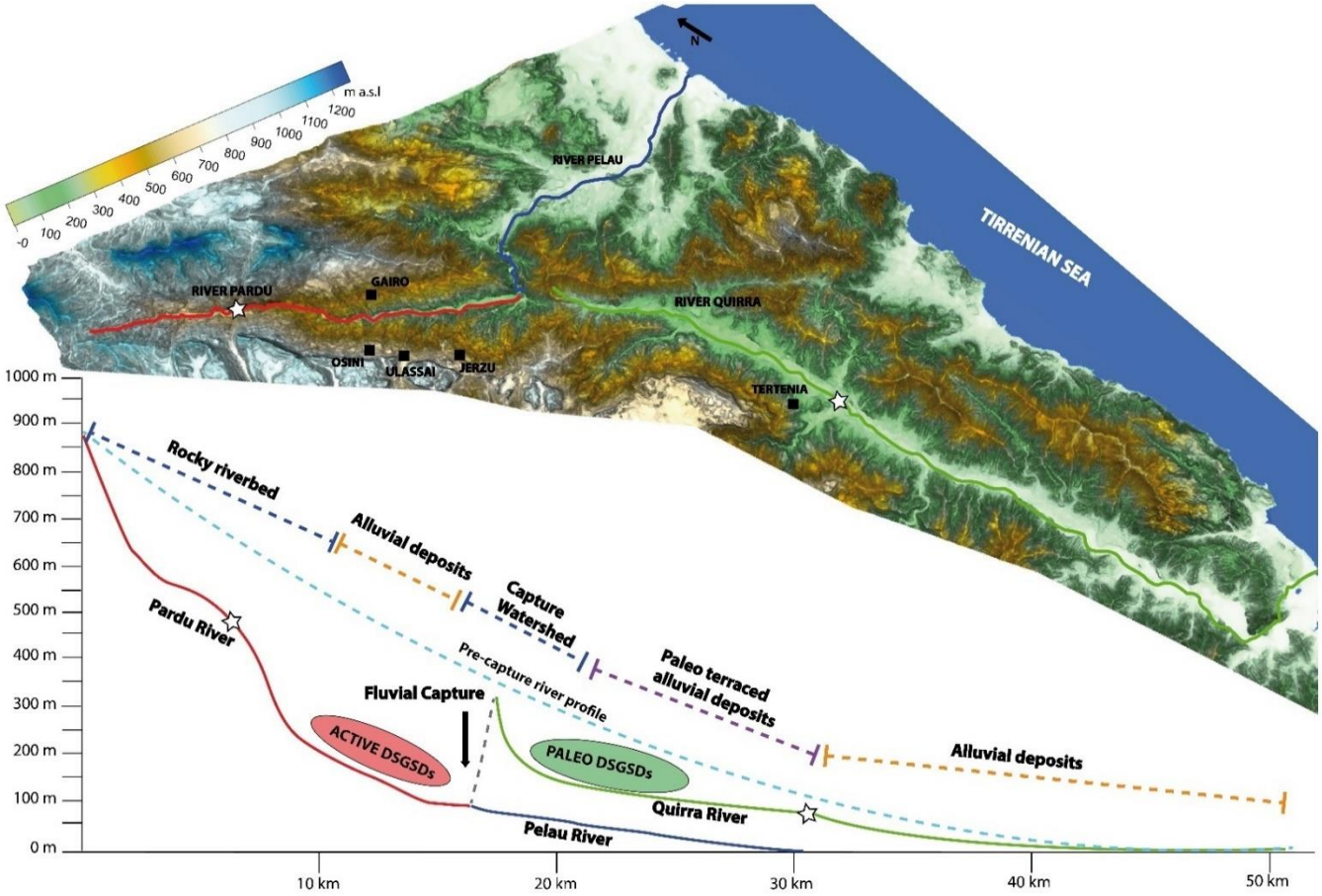


**Figure 14.** Relation between DGSD activity and river parameters.

These DGSDs were associated with numerous large collateral rockfalls and toppling landslides that affected the slopes. Dolomitic blocks with sizes of up to 30 m on each side were identified; these moved up to 900 m away from the detachment points, which were linked to mega-rockfall events with rock avalanche features. We also identified paleo-

DGSDs on the downslope that were associated with the collapsed slope side. Currently, a reactivation of quiescent DGSDs or an acceleration of movements can be triggered by extreme weather events or earthquakes.

Therefore, an acceleration of slope movements leading to a potential catastrophic failure poses a threat to communities, and the monitoring of these slopes is important for early warning and risk reduction. So, we studied the DGSDs and landslides in the inhabited areas of Pardu Valley in detail by using integrated remote sensing techniques, field mapping, and InSAR in order to understand the temporal evolution. The historical InSAR deformation rate supports our model of rock slope deformation. However, for risk reduction in a populated area, a 24/7 monitoring system could become an essential component of an early-warning system that is aimed at preparing evacuation protocols [55,111–118].

## 8. Conclusions

The connection between Plio-Pleistocenic tectonic activity and geomorphological evolution in the Pardu Valley and Quirra Valley (Ogliastra, East Sardinia) was studied. The evolutionary conditions of the Pardu Valley are associated with a cycle of undeveloped fluvial erosion, which suggests a relatively young age of the engraving in relation to the capture by the Rio Pelau and the isolation of the Rio Quirra. The intense post-capture erosion has given the Rio Pardu Valley morphometric features that are favorable for the evolution of DGSDs. However, the Rio Quirra Valley presents paleo-DGSDs that have been fossilized by pre-capture terraced alluvial deposits.

The DGSDs' movements are linked to the recent tectonic evolution (areal uplift). The two valleys analyzed are controlled by transcurrent faults that have recently recorded low-magnitude seismic events. Therefore, it is possible that the constant movement of the DGSDs (between about 1 and 2 cm/y) may be susceptible to accelerations due to seismic triggering, causing the partial collapse of the slopes.

In particular, this research highlighted the following:

- The geomorphological and structural setting of Ogliastra is closely linked to the genesis of the east Sardinian continental margin due the opening of the Tyrrhenian basin (Miocene–Pliocene)
- Distensive Pliocene tectonics accompanied by widespread volcanism resulted in a general uplift in Sardinia. The Quaternary uplift rebound manifested itself with an important erosive phase and variations in the hydrographic network. We have evidence of this phase in the Rio Quirra Valley, which is represented by paleo-DGSDs fossilized by pre-Tyrrhenian alluvial deposits (Lower Pleistocene).
- The river capture of Rio Pardu is associated with this important erosive phase and caused an erosive increase that led to a complete emptying of the valley (Upper-Middle Pleistocene).
- The post-capture decompression of the slopes of the Rio Pardu triggered DGSDs in both flanks in the current state of activity.
- Using InSAR data, it was possible to identify and assign displacement rates to the Ulassai, Osini, and Gairo DGSDs.

**Author Contributions:** Conceptualization, V.D., P.E.O. and G.D.; methodology, V.D. and G.D.; validation, P.E.O.; formal analysis, V.D.; investigation, V.D., P.E.O. and G.D.; resources, P.E.O. and G.D.; data curation, V.D.; writing—original draft preparation, V.D.; writing—review and editing, V.D., P.E.O. and G.D.; visualization, V.D., P.E.O. and G.D.; supervision, G.D. and P.E.O.; project administration, P.E.O.; funding acquisition, P.E.O. All authors have read and agreed to the published version of the manuscript.

**Funding:** Valentino Demurtas acknowledges the support from the University of Cagliari—Dottorato di Ricerca XXXIV ciclo—Earth and Environmental Sciences and Technologies.

**Institutional Review Board Statement:** Not applicable.

**Informed Consent Statement:** Not applicable.

**Data Availability Statement:** Not applicable.

**Acknowledgments:** We are thankful to Reginald Hermanns for the precious suggestions. We are also grateful to Marie Bredal for the technical support in the InSAR processing. The precious contributions of the two anonymous reviewers and of the journal editors are acknowledged.

**Conflicts of Interest:** The authors declare no conflict of interest.

## References

1. Carmignani, L.; Oggiano, G.; Barca, S.; Conti, P.; Salvadori, I.; Eltrudis, A.; Funedda, A.; Pasci, S. Geologia della Sardegna: Note Illustrative della Carta Geologica della Sardegna in scala 1:200.000. In *Memorie Descrittive della Carta Geologica d'Italia*; ISPRA—Servizio Geologico d'Italia: Rome, Italy, 2001; Volume 60.
2. Carminati, E.; Doglioni, C. Mediterranean tectonics. In *Encyclopedia of Geology*; Selley, R., Cocks, R., Plimer, I., Eds.; Elsevier: Amsterdam, The Netherlands, 2005; pp. 135–146.
3. Cherchi, A.; Montadert, L. Oligo-Miocene rift of Sardinia and the early history of the Western Mediterranean Basin. *Nature* **1982**, *298*, 736–739. [CrossRef]
4. Maxia, C.; Ulzega, A.; Marini, C. Studio idrogeologico dei dissesti nel bacino del Rio Pardu (Sardegna centro-orientale). *Pubblicazione dell'Istituto di Geologia, Paleontologia e Geografia Fisica* **1973**, *12*, 1–9.
5. Ulzega, A.; Marini, A. L'évolution des versants dans la vallée du Rio Pardu (Sardaigne centre-orientale). *Zeitschrift fur Geomorphologie* **1973**, *21*, 466–474.
6. Demurtas., V.; Orrù, P.E.; Deiana, G. Deep-seated gravitational slope deformations in central Sardinia: Insights into the geomorphological evolution. *J. Maps* **2021**, *17*, 594–607.
7. De Waele, J.; Ferrarese, F.; Granger, D.; Sauro, F. Landscape evolution in the Tacchi area (central-east Sardinia, Italy) based on karst and fluvial morphology and age of cave sediments. *Geografia Fisica e Dinamica Quaternaria* **2012**, *35*, 119–127. [CrossRef]
8. Deiana, G.; Lecca, L.; Melis, R.T.; Soldati, M.; Demurtas, V.; Orrù, P.E. Submarine geomorphology of the southwestern Sardinian continental shelf (Mediterranean Sea): Insights into the last glacial maximum sea-level changes and related environments. *Water* **2021**, *13*, 155. [CrossRef]
9. Suhail, H.A.; Yang, R.; Chen, H.; Rao, G. The impact of river capture on the landscape development of the Dadu River drainage basin, eastern Tibetan plateau. *J. Asian Earth Sci.* **2020**, *198*, 1367–9120. [CrossRef]
10. Carabella, C.; Buccolini, M.; Galli, L.; Miccadei, E.; Paglia, G.; Piacentini, T. Geomorphological analysis of drainage changes in the NE Apennines piedmont area: The case of the middle Tavo River bend (Abruzzo, central Italy). *J. Maps* **2020**, *16*, 222–235. [CrossRef]
11. Fan, N.; Chu, Z.; Jiang, L. Abrupt drainage basin reorganization following a Pleistocene river capture. *Nat. Commun.* **2018**, *9*, 3756. [CrossRef]
12. Bishop, P. Drainage rearrangement by river capture, beheading and diversion. *Prog. Phys. Geogr.* **1995**, *19*, 449–473. [CrossRef]
13. Willett, S.D.; McCoy, S.W.; Perron, J.T.; Goren, L.; Chen, C.Y. Dynamic reorganization of river basins. *Science* **2014**, *343*, 1117.
14. Whipple, K.X.; Forte, A.M.; Di Biase, R.A. Timescales of landscape response to divide migration and drainage capture: Implications for the role of divide mobility in landscape evolution. *J. Geophys. Res. Earth Surf.* **2017**, *122*, 248–273.
15. Prince, P.S.; Spotila, J.A.; Henika, W.S. Stream capture as driver of transient landscape evolution in a tectonically quiescent setting. *Geology* **2011**, *39*, 823–826.
16. Aslan, A.; Hood, W.C.; Karlstrom, K.E.; Kirby, E.; Granger, D.E.; Kelley, S.; Asmerom, Y. Abandonment of Unaweep Canyon (1.4–0.8 Ma), western Colorado: Effects of stream capture and anomalously rapid Pleistocene river incision. *Geosphere* **2014**, *10*, 428–446. [CrossRef]
17. Shugar, D.; Clague, J.; Best, J.; Schoof, C.; Willis, M.; Copland, L.; Roe, G. River piracy and drainage basin reorganization led by climate-driven glacier retreat. *Nat. Geosci.* **2017**, *10*, 370–375. [CrossRef]
18. Bracciali, L.; Najman, Y.; Parrish, R.R.; Akhter, S.H.; Millar, I. The Brahmaputra tale of tectonics and erosion: Early Miocene river capture in the Eastern Himalaya. *Earth Planet. Sci. Lett.* **2015**, *415*, 25–37. [CrossRef]
19. Antón, L.; De Vicente, G.; Munoz-Martin, A.; Stokes, M. Using river long profiles and geomorphic indices to evaluate the geomorphological signature of continental scale drainage capture, Duero basin (NW Iberia). *Geomorphology* **2014**, *206*, 250–261. [CrossRef]
20. Pánek, T.; Šilhán, K.; Tábořík, P.; Hradecký, J.; Smolková, V.; Lenart, J.; Pazdur, A. Catastrophic slope failure and its origins: Case of the May 2010 Girová Mountain long-runout rockslide (Czech Republic). *Geomorphology* **2011**, *130*, 352–364. [CrossRef]
21. Quesada-Román, A.; Fallas-López, B.; Hernández-Espinoza, K.; Stoffel, M.; Ballesteros-Cánovas, J.A. Relationships between earthquakes, hurricanes, and landslides in Costa Rica. *Landslides* **2019**, *16*, 1539–1550. [CrossRef]
22. Volpe, E.; Ciabatta, L.; Salciarini, D.; Camici, S.; Cattoni, E.; Brocca, L. The impact of probability density functions assessment on model performance for slope stability analysis. *Geosciences* **2021**, *11*, 322.
23. Shou, K.J.; Chen, J. On the rainfall induced deep-seated and shallow landslide hazard in Taiwan. *Eng. Geol.* **2021**, *288*, 106156. [CrossRef]
24. Quesada-Román, A. Landslide risk index map at the municipal scale for Costa Rica. *Int. J. Disaster Risk Reduct.* **2021**, *56*, 102144. [CrossRef]

25. Marini, A.; Ulzega, A. Osservazioni geomorfologiche sul tacco di ulassai. *Rendiconti Seminario Facoltà Scienze Università di Cagliari* **1977**, *47*, 192–208.
26. Proggetto AVI Aree Vulnerate Italiane. Available online: http://avi.gndci.cnr.it/ (accessed on 1 September 2020).
27. Moretti, A. Sui movimenti franosi degli abitati di Osini e di Gairo (Nuoro). *Bollettino del Servizio Geologico d'Italia* **1953**, *75*, 2.
28. Zischinsky, U. On the deformation of high slopes. In Proceedings of the 1st Conference International Society for RockMechanics, Lisbon, Portugal, 25 September–1 October 1966; Volume 2, pp. 179–185.
29. Zischinsky, U. Über Sackungen. *Rock Mech.* **1969**, *1*, 30–52. [CrossRef]
30. Radbruch-Hall, D.; Varnes, D.J.; Savage, W.Z. Gravitational spreading of steep-sided ridges ("sackung") in western United States. *Bull. Int. Assoc. Eng. Geol.* **1976**, *13*, 23–35. [CrossRef]
31. Radbruch-Hall, D. Gravitational creep of rock masses on slopes. In *Rockslides and Avalanches—Natural Phenomena: Developments in Geotechnical Engineering*; Voight, B., Ed.; Elsevier: Amsterdam, The Netherlands, 1978; Volume 14, pp. 607–658.
32. Bisci, C.; Dramis, F.; Sorriso-Valvo, M. Rock flow (sackung). In *Landslide Recognition: Identification, Movement and Causes*; Dikau, R., Brunsden, D., Schrott, L., Ibsen, M.L., Eds.; John Wiley & Sons, Inc.: Hoboken, NJ, USA, 1996; pp. 150–160.
33. Jahn, A. Slope morphological feature resulting from gravitation. *Z. Für Geomorphol.* **1964**, *5*, 59–72.
34. Cruden, D.M.; Varnes, D.J. Landslide Types and Processes. *Spec. Rep. Natl. Res. Counc. Transp. Res. Board* **1996**, *247*, 36–75.
35. Pasuto, A.; Soldati, M. Lateral spreading. In *Landslide Recognition: Identification, Movement and Causes*; Dikau, R., Brunsden, D., Schrott, L., Ibsen, M.-L., Eds.; John Wiley & Sons, Inc.: Hoboken, NJ, USA, 1996; pp. 122–136.
36. Dramis, F.; Sorriso-Valvo, M. Deep-seated gravitational slope deformations, related landslides and tectonics. *Eng. Geol.* **1994**, *38*, 231–243. [CrossRef]
37. Dramis, F.; Farabollini, P.; Gentili, B.; Pambianchi, G. Neotectonics and large scale gravitational phenomena in the Umbria –Marche Apennines, Italy. In *Seismically Induced Ground Ruptures and Large Scale Mass Movements, Field Excursion and Meeting*; Comerci, V., D'Agostino, N., Fubelli, G., Molin, P., Piacentini, T., Eds.; APAT: Rome, Italy, 2002; Volume 21, pp. 17–30.
38. Agliardi, F.; Scuderi, M.M.; Fusi, N.; Cristiano, C. Slow-to-fast transition of giant creeping rockslides modulated by undrained loading in basal shear zones. *Nat. Commun.* **2020**, *11*, 1352. [CrossRef]
39. Crosta, G.B.; Agliardi, F. Failure forescast for large rock slides by surface displacement measurements. *Can. Geotech. J.* **2003**, *40*, 176–191. [CrossRef]
40. Nemčok, A. Gravitational slope deformation in high mountains. In Proceedings of the 24th International Geology Congress, Montreal, QC, Canada, 1972; Volume 13, pp. 132–141.
41. Ostermann, M.; Sanders, D. The Benner pass rock avalanche cluster suggests a close relation between long-term slope deformation (DSGSDs and translational rock slides) and catastrophic failure. *Geomorphology* **2017**, *289*, 44–59. [CrossRef]
42. Soldati, M. Deep-seated gravitational slope deformation. In *Encyclopedia of Natural Hazards*; Bobrowsky, P.T., Ed.; Encyclopedia of Earth Sciences Series; Springer: Berlin/Heidelberg, Germany, 2013.
43. Agliardi, F.; Crosta, G.; Zanchi, A. Structural constraints on deep seated slope deformation kinematics. *Eng. Geol.* **2001**, *59*, 83–102. [CrossRef]
44. Chigira, M. Long-term gravitational deformation of rocks by mass rock creep. *Eng. Geol.* **1992**, *32*, 157–184. [CrossRef]
45. Crosta, G.B.; Frattini, P.; Agliardi, F. Deep seated gravitational slope deformations in the European Alps. *Tectonophysics* **2013**, *605*, 13–33. [CrossRef]
46. Mariani, G.S.; Zerboni, A. Surface geomorphological features of deep-seated gravitational slope deformations: A look to the role of lithostructure (N Apennines, Italy). *Geosciences* **2020**, *10*, 334. [CrossRef]
47. Pánek, T.; Klimeš, J. Temporal behavior of deep-seated gravitational slope deformations: A review. *Earth-Sci. Rev.* **2016**, *156*, 14–38. [CrossRef]
48. Crosta, G.B.; Zanchi, A. Deep-seated slope deformations. Huge, extraordinary, enigmatic phenomena. In *Landslides in Research, Theory and Practice*; Bromhead, E., Dixon, N., Ibsen, M., Eds.; Thomas Telford Ltd.: London, UK, 2000; pp. 351–358.
49. Gentili, B.; Pambianchi, G. Gravitational morphogenesis of the Apennine chain in Central Italy. In Proceedings of the 7th International Congress International Association of Engineering Geology, Lisboa, Portugal, 5–9 September 1994; Volume 3, pp. 1177–1186.
50. Iovine, G.; Tansi, C. Gravity-accommodated 'structural wedges' along thrust ramps: A kinematic scheme of gravitational evolu-tion. *Nat. Hazards* **1998**, *17*, 195–224. [CrossRef]
51. Frigerio, S.; Schenato, L.; Bossi, G.; Cavalli, M.; Mantovani, M.; Marcato, G.; Pasuto, A. A web-based platform for automatic and continuous landslide monitoring: The Rotolon (Eastern Italian Alps) case study. *Comput. Geosci.* **2014**, *63*, 96–105.
52. Sestras, P.; Bilașco, Ș.; Roșca, S.; Dudic, B.; Hysa, A.; Spalević, V. Geodetic and UAV monitoring in the sustainable management of shallow landslides and erosion of a susceptible urban environment. *Remote Sens.* **2021**, *13*, 385.
53. Zhang, L.; Wang, X.; Xia, T.; Yang, B.; Yu, B. Deformation characteristics of Tianjiaba landslide induced by surcharge. *ISPRS Int. J. Geo-Inf.* **2021**, *10*, 221. [CrossRef]
54. Bianchini, S.; Solari, L.; Bertolo, D.; Thuegaz, P.; Catani, F. Integration of satellite interferometric data in civil protection strategies for landslide studies at a regional scale. *Remote Sens.* **2021**, *13*, 1881. [CrossRef]
55. Demurtas, V.; Orrù, P.; Deiana, G. Multi-source and multi-scale monitoring system of deep-seated gravitational slope deformation in east-central sardinia. *Planet Care Space* **2021**, *2*, 28–32. [CrossRef]

56. Carmignani, L.; Oggiano, G.; Funedda, A.; Conti, P.; Pasci, S. The geological map of Sardinia (Italy) at 1:250,000 scale. *J. Maps* **2016**, *12*, 826–835. [CrossRef]
57. Pertusati, P.C.; Sarria, E.; Cherchi, G.P.; Carmignani, L.; Barca, S.; Benedetti, M.; Chighine, G.; Cincotti, E.; Oggiano, G.; Ulzega, A.; et al. *Geological Map of Italty. Scale 1:50.000*; Scheet 541 "Jerzu"; ISPRA-Servizio Geologico Nazionale: Rome, Italy, 2002.
58. Chiocci, F.L.; Budillon, F.; Ceramicola, S.; Gamberi, F.; Orrù, P. *A Tlante dei Lineamenti di Pericolosità Geologica dei Mari Italiani-Risultati del Progetto MaGIC*; CNR Edizioni: Rome, Italy, 2021.
59. Carmignani, L.; Carosi, R.; Di Pisa, A.; Gattiglio, G.; Musumeci, G.; Oggiano, G.; Pertusati, P.C. The Hercynian chain in Sardinia (Italy). *Geodin. Acta* **1994**, *7*, 31–47. [CrossRef]
60. Elter, F.M.; Corsi, B.; Cricca, P.; Muzio, G. The south-western Alpine foreland: Correlation between two sectors of the Variscan chain belonging to "stable Europe": Sardinia (Italy) Corsica and Maures Massif (south-eastern France). *Geodin. Acta* **2004**, *17*, 31–40. [CrossRef]
61. Elter, F.M.; Padovano, M.; Kraus, R.K. The emplacement of Variscan HT metamorphic rocks linked to the interaction between Gondwana and Laurussia: Structural constraints in NE Sardinia (Italy). *Terra Nova* **2010**, *22*, 369–377. [CrossRef]
62. Meloni, M.A.; Oggiano, G.; Funedda, A.; Pistis, M.; Linnemann, U. Tectonics, ore bodies, and gamma-ray logging of the Variscan basement, southern Gennargentu massif (central Sardinia, Italy). *J. Maps* **2017**, *13*, 196–206. [CrossRef]
63. Vai, G.B.; Cocozza, T. II "postgotlandiano" sardo, unità sinorogenica ercinica. *Boll. Della Soc. Geol. Ital.* **1974**, *93*, 61–72.
64. Costamagna, L.G.; Barca, S. Stratigraphy, facies analysis, paleogeography and regional framework of the Jurssic succession of the "tacchi" area (Middle-Eastern Sardinia). *Bollettino della Societa Geologica Italiana* **2004**, *123*, 477–495.
65. Marini, C. Le concentrazioni residuali post-erciniche di Fe dell'Ogliastra (Sardegna orientale): Contesto geologico e dati mineralogici. *Rendiconti della Societa Italiana di Mineralogia e Petrologia* **1984**, *39*, 229–238.
66. Costamagna, L.G.; Kustatscher, E.; Scanu, G.G.; Del Rio, M.; Pittau, P.; Van Konijnenburg-van Cittert, J.H.A. A palaeoenvironmental reconstruction of the Middle Jurassic of Sardinia (Italy) based on integrated palaeobotanical, palynological and lithofacies data assessment. *Palaeobiodivers. Palaeoenviron.* **2018**, *98*, 111–138. [CrossRef]
67. Dieni, I.; Fischer, J.C.; Massari, F.; Salard-Cheboldaeff, M.; Vozenin-Serra, C. La succession de Genna Selole (Baunei) dans le cadre de la paléogéographie mésojurassique de la Sardaigne orientale. *Memorie della Società Geologica Italiana* **1983**, *36*, 117–148.
68. Costamagna, L.G. Middle Jurassic continental to marine transition in an extensional tectonics context: The Genna Selole Fm depositional system in the Tacchi area (central sardinia. Italy). *Geol. J.* **2015**, *51*, 722–736. [CrossRef]
69. Gattacceca, J.; Deino, A.; Rizzo, R.; Jones, D.S.; Henry, B.; Beaudoin, B.; Vadeboin, F. Miocene rotation of Sardinia: New paleomagnetic and geochronological constraints and geodynamic implications. *Earth Planet Sci. Lett.* **2007**, *258*, 359–377. [CrossRef]
70. Ulzega, A.; Orrù, P.E.; Pintus, C.; Pertusati, P.C.; Sarria, E.; Cherchi, G.P.; Carmignani, L.; Barca, S.; Benedetti, M.; Chighine, G.; et al. *Geological Map of Italty. Scale 1:50.000*; Scheet 541 "Jerzu"; ISPRA-Servizio Geologico Nazionale: Rome, Italy, 2002.
71. Gueguen, E.; Doglioni, C.; Fernandez, M. Lithospheric boudinage in the Western Mediterranean back-arc basin. *Terra Nova* **1997**, *9*, 184–187. [CrossRef]
72. Oggiano, G.; Funedda, A.; Carmignani, L.; Pasci, S. The Sardinia-Corsica microplate and its role in the northern Apennine geodynamics: New insights from the tertiary intraplate strike-slip tectonics of Sardinia. *Ital. J. Geosci.* **2009**, *128*, 527–541. [CrossRef]
73. Casula, G.; Cherchi, A.; Montadert, L.; Murru, M.; Sarria, E. The cenozoic graben system of Sardinia (Italy): Geodynamic evolution from new seismic and field data. *Mar. Pet. Geol.* **2001**, *18*, 863–888. [CrossRef]
74. Lustrino, M.; Melluso, L.; Morra, V. The geochemical peculiarity of Plio-Quaternary volcanic rocks of Sardinia in the circum-Mediterranean area. *Geol. Soc. Am.* **2007**, *418*, 277–301.
75. Marini, A.; Murru, M. Movimenti tettonici in Sardegna fra il Miocene Superiore ed il Pleistocene. *Geografia Fisica e Dinamica Quaternaria* **1983**, *6*, 39–42.
76. Ferranti, L.; Oldow, J.S.; D'Argenio, B.; Catalano, R.; Lewis, D.; Marsella, E.; Avellone, G.; Maschio, L.; Pappone, G.; Pepe, F.; et al. Active deformation in southern Italy, Sicily and southern Sardinia from GPS velocities of the Peri-Tyrrhenian Geodetic Array (PTGA). *Boll. Soc. Geol. Ital.* **2008**, *127*, 299–316.
77. Cimini, G.B.; Marchetti, A.; Silvestri, M. *L'esperimento Sardinia Passive Array (spa): Acquisizione Dati Sismici Per lo Studio Della Geodinamica e Della Sismotettonica Dell'area Mediterranea*; Istituto Nazionale di Geofisica e Vulcanologia, Centro Nazionale Terremoti (INGV): Rome, Italy, 2016.
78. INGV. INGV Special, the Earthquakes of 2020 in Italy. 2021. Available online: http://terremoti.ingv.it/ (accessed on 30 September 2021).
79. Palomba, M.; Ulzega, A. Geomorfologia dei depositi quaternari del Rio Quirra e della piattaforma continentale antistante (Sardegna Orientale). *Rendiconti Saminario Facoltà Scienze Università Cagliari* **1984**, *54*, 109–121.
80. De Waele, J.; Di Gregorio, F.; Follesa, R.; Piras, G. Geosites and landscape evolution of the "tacchi": An example from central-east Sardinia. *II Quaternario* **2005**, *18*, 211–220.
81. Fleurant, C.; Tucker, G.E.; Viles, H.A. A model of cockpit karst landscape, Jamaica. In *Géomorphologie: Relief, Processus, Environnement*; Groupe Français de Géomorphologie: Paris, France, 2008; pp. 3–14.
82. Liang, F.; Xu, B. Discrimination of tower-, cockpit-, and non-karst landforms in Guilin, southern China, based on morphometric characteristics. *Geomorphology* **2014**, *204*, 42–48. [CrossRef]

83. Waltham, T. Fengcong, fenglin, cone karst and tower karst. *Cave Karst Sci.* **2008**, *35*, 77–88.
84. Gamberi, F.; Leidi, E.; Dalla Valle, G.; Rovere, M.; Marani, M.; Mercorella, A. Foglio 57 Arbatax. In *A Tlante dei Lineamenti di Pericolosità Geologica dei Mari Italiani-Risultati del Progetto MaGIC*; Chiocci, F.L., Budillon, F., Ceramicola, S., Gamberi, F., Orrù, P., Eds.; CNR Edizioni: Rome, Italy, 2021.
85. Marani, M.; Gamberi, F. Structural framework of the Tyrrhenian Sea unveiled by seafloor morphology. In *From Seafloor to Deep Mantle: Architecture of the Tyrrhenian Backarc Basin*; Memorie Descrittive della Carta Geolologica d'Italia; Marani, M., Gamberi, F., Bonatti, E., Eds.; ISPRA: Rome, Italy, 2004; Volume 44, pp. 97–108.
86. ISPRA & AIGEO. *Aggiornamento ed Integrazione Delle linee Guida Della Carta Geomorfologica d'Italia in Scala 1:50,000*; Quaderni Serie III del; Servizio Geologico Nazionale: Rome, Italy, 2018.
87. Miccadei, E.; Carabella, C.; Paglia, G.; Piacentini, T. Paleo-drainage network, morphotectonics, and fluvial terraces: Clues from the verde stream in the Middle Sangro River (central Italy). *Geosciences* **2018**, *8*, 337. [CrossRef]
88. Miccadei, E.; Carabella, C.; Paglia, G. Morphoneotectonics of the Abruzzo Periadriatic area (central Italy): Morphometric analysis and morphological evidence of tectonics features. *Geosciences* **2021**, *11*, 397. [CrossRef]
89. Guzzetti, F.; Carrara, A.; Cardinali, M.; Reichenbach, P. Landslide hazard evaluation: A review of current techniques and their application in a multi-scale study, central Italy. *Geomorphology* **1999**, *31*, 181–216. [CrossRef]
90. Dragićević, S.; Lai, T.; Balram, S. GIS-based multicriteria evaluation with multiscale analysis to characterize urban landslide susceptibility in data-scarce environments. *Habitat Int.* **2015**, *45*, 114–125.
91. Shi, W.; Deng, S.; Xu, W. Extraction of multi-scale landslide morphological features based on local Gi* using airborne LiDAR-derived DEM. *Geomorphology* **2018**, *303*, 229–242.
92. Yi, Y.; Zhang, Z.; Zhang, W.; Jia, H.; Zhang, J. Landslide susceptibility mapping using multiscale sampling strategy and convolutional neural network: A case study in Jiuzhaigou region. *Catena* **2020**, *195*, 104851.
93. Deiana, G.; Melis, M.T.; Funedda, A.; Da Pelo, S.; Meloni, M.; Naitza, L.; Orrù, P.; Salvini, R.; Sulis, A. Integrating remote sensing data for the assessments of coastal cliffs hazard: MAREGOT project. *Earth Obs. Adv. Chang. World* **2019**, *1*, 176–181.
94. Melis, M.T.; Da Pelo, S.; Erbì, I.; Loche, M.; Deiana, G.; Demurtas, V.; Meloni, M.A.; Dessì, F.; Funedda, A.; Scaioni, M.; et al. Thermal remote sensing from UAVs: A review on methods in coastal cliffs prone to landslides. *Remote Sens.* **2020**, *12*, 1971. [CrossRef]
95. Devoto, S.; Macovaz, V.; Mantovani, M.; Soldati, M.; Furlani, S. Advantages of using UAV digital photogrammetry in the study of slow-moving coastal landslides. *Remote Sens.* **2020**, *12*, 3566.
96. Gaidi, S.; Galve, J.P.; Melki, F.; Ruano, P.; Reyes-Carmona, C.; Marzougui, W.; Devoto, S.; Pérez-Peña, J.V.; Azañón, J.M.; Chouaieb, H.; et al. Analysis of the geological controls and kinematics of the chgega landslide (Mateur, Tunisia) exploiting photogrammetry and InSAR technologies. *Remote Sens.* **2021**, *13*, 4048. [CrossRef]
97. Delgado, J.; Vicente, F.; García-Tortosa, F.; Alfaro, P.; Estévez, A.; Lopez-Sanchez, J.M.; Tomás, R.; Mallorquí, J.J. A deep seated compound rotational rock slide and rock spread in SE Spain: Structural control and DInSAR monitoring. *Geomorphology* **2011**, *129*, 252–262. [CrossRef]
98. Oliveira, S.C.; Zêzere, J.L.; Catalão, J.; Nico, G. The contribution of PSInSAR interferometry to landslide hazard in weak rock-dominated areas. *Landslides* **2015**, *12*, 703–719. [CrossRef]
99. Crosetto, M.; Monserrat, O.; Cuevas-González, M.; Devanthéry, N.; Crippa, B. Persistent scatterer interferometry: A review. *ISPRS J. Photogramm. Remote Sens.* **2016**, *115*, 78–89. [CrossRef]
100. Mantovani, M.; Devoto, S.; Piacentini, D.; Prampolini, M.; Soldati, M.; Pasuto, A. Advanced SAR interferometric analysis to support geomorphological interpretation of slow-moving coastal landslides (Malta, Mediterranean Sea). *Remote Sens.* **2016**, *8*, 443. [CrossRef]
101. Frattini, P.; Crosta, G.B.; Rossini, M.; Allievi, J. Activity and kinematic behaviour of deep-seated landslides from PS-InSAR displacement rate measurements. *Landslides* **2018**, *15*, 1053–1070. [CrossRef]
102. Novellino, A.; Cesarano, M.; Cappelletti, P.; Di Martire, D.; Di Napoli, M.; Ramondini, M.; Sowter, A.; Calcaterra, D. Slow-moving landslide risk assessment combining machine learning and InSAR techniques. *Catena* **2021**, *203*, 105317. [CrossRef]
103. Eker, R.; Aydın, A. Long-term retrospective investigation of a large, deep-seated, and slow-moving landslide using InSAR time series, historical aerial photographs, and UAV data: The case of Devrek landslide (NW Turkey). *Catena* **2021**, *196*, 104895. [CrossRef]
104. Peternal, T.; Kumelj, S.; Ostir, K.; Komac, M. Monitoring the Potoška planina landslide (NW Slovenia) using UAV photogrammetry and tachymetric measurements. *Landslides* **2017**, *14*, 395–406. [CrossRef]
105. Valkaniotis, S.; Papathanassiou, G.; Ganas, A. Mapping an earthquake-induced landslide based on UAV imagery; case study of the 2015 Okeanos landslide, Lefkada, Greece. *Eng. Geol.* **2018**, *245*, 141–152. [CrossRef]
106. Clapuyt, F.; Vanacker, V.; Oost, K.V. Reproducibility of UAV-based earth topography reconstructions based on structure-from-motion algorithms. *Geomorphology* **2016**, *260*, 4–15. [CrossRef]
107. Ietto, F.; Perri, F.; Fortunato, G. Lateral spreading phenomena and weathering processes from the Tropea area (Calabria, southern Italy). *Environ. Earth Sci.* **2015**, *73*, 4595–4608. [CrossRef]
108. Mateos, R.M.; Ezquerro, P.; Azañón, J.M.; Gelabert, B.; Herrera, G.; Fernández-Merodo, J.A.; Spizzichino, D.; Sarro, R.; Garcia-Moreno, I.; Bejar-Pizarro, M. Coastal lateral spreading in the world heritage site of the Tramuntana Range (Majorca, Spain). The use of PSInSAR monitoring to identify vulnerability. *Landslides* **2018**, *15*, 797–809. [CrossRef]

109. Moretto, S.; Bozzano, F.; Mazzanti, P. The role of satellite InSAR for landslide forecasting: Limitations and openings. *Remote Sens.* **2021**, *13*, 3735. [CrossRef]
110. Mondini, A.C.; Guzzetti, F.; Chang, K.-T.; Monserrat, O.; Martha, T.R.; Manconi, A. Landslide failures detection and mapping using synthetic aperture radar: Past, present and future. *Earth-Sci. Rev.* **2021**, *216*, 103574.
111. Zhang, Y.; Li, H.; Sheng, Q.; Wu, K.; Chen, G. Real time remote monitoring and pre-warning system for highway landslide in mountain area. *J. Environ. Sci. China* **2011**, *23*, S100–S105.
112. Barla, G.; Antolini, F.; Barla, M.; Mensi, E.; Piovano, G. Monitoring of the Beauregard landslide (Aosta Valley, Italy) using advanced and conventional techniques. *Eng. Geol.* **2010**, *116*, 218–235.
113. Intrieri, E.; Gigli, G.; Mugnai, F.; Fanti, R.; Casagli, N. Design and implementation of a landslide early warning system. *Eng. Geol.* **2012**, *147*, 124–136.
114. Naidu, S.; Sajinkumar, K.S.; Oommen, T.; Anuja, V.J.; Samuel, R.A.; Muraleedharan, C. Early warning system for shallow landslides using rainfall threshold and slope stability analysis. *Geosci. Front.* **2018**, *9*, 1871–1882. [CrossRef]
115. Piciullo, L.; Calvello, M.; Cepeda, J.M. Territorial early warning systems for rainfall-induced landslides. *Earth-Sci. Rev.* **2018**, *179*, 228–247.
116. Guzzetti, F.; Gariano, S.L.; Peruccacci, S.; Brunetti, M.T.; Marchesini, I.; Rossi, M.; Melillo, M. Geographical landslide early warning systems. *Earth-Sci. Rev.* **2020**, *200*, 102973. [CrossRef]
117. Xu, Q.; Peng, D.; Zhang, S.; Zhu, X.; He, C.; Qi, X.; Zhao, K.; Xiu, D.; Ju, N. Successful implementations of a real-time and intelligent early warning system for loess landslides on the Heifangtai terrace, China. *Eng. Geol.* **2020**, *278*, 105817. [CrossRef]
118. Tzouvaras, M. Statistical time-series analysis of interferometric coherence from sentinel-1 sensors for landslide detection and early warning. *Sensors* **2021**, *21*, 6799. [CrossRef]